Variability in magnitude of paleoearthquakes revealed by trenching and historical records, along the Haiyuan Fault, China

Jing Liu-Zeng, Yanxiu Shao, Yann Klinger, Kejia Xie, Daoyuang Yuan, Zhongsheng Lei

AGU PUBLICATIONS

JGR

Journal of Geophysical Research: Solid Earth

RESEARCH ARTICLE
10.1002/2015JB012163

Key Points:
- Historical accounts suggest paleoearthquakes of markedly different magnitudes
- Moderate-magnitude events can be preserved in stratigraphy

Correspondence to:
J. Liu-Zeng,
liu-zeng@ies.ac.cn

Citation:
Liu-Zeng, J., Y. Shao, Y. Klinger, K. Xie, D. Yuan, and Z. Lei (2015), Variability in magnitude of paleoearthquakes revealed by trenching and historical records, along the Haiyuan Fault, China, *J. Geophys. Res. Solid Earth*, *120*, 8304–8333, doi:10.1002/2015JB012163.

Received 30 APR 2015
Accepted 25 OCT 2015
Accepted article online 27 OCT 2015
Published online 2 DEC 2015

Variability in magnitude of paleoearthquakes revealed by trenching and historical records, along the Haiyuan Fault, China

Jing Liu-Zeng[1], Yanxiu Shao[1,2], Yann Klinger[3], Kejia Xie[1], Daoyuang Yuan[2], and Zhongsheng Lei[2]

[1]State Key Laboratory of Earthquake Dynamics, Institute of Geology, China Earthquake Administration, Beijing, China, [2]Lanzhou Institute of Seismology, China Earthquake Administration, Lanzhou, China, [3]Institut de Physique du Globe, Sorbonne Paris Cité, Université Paris Diderot, UMR 7154 CNRS, Paris, France

Abstract Paleoseismology provides fundamental data for generalizing earthquake recurrence behavior, by revealing past surface-rupturing events. Determining the size of paleoseismic events is notoriously more challenging than their timing. Paleoearthquakes exposed in trenches are vaguely defined as large enough to break to the surface and often assumed to be similar in size. Here we show an example where the paleoseismic record includes events of both moderate and large magnitudes. At the Salt Lake site on the active left-lateral Haiyuan Fault, northern Tibetan Plateau, a high-resolution stratigraphic sequence recorded three and possibly four events since A.D. 1500, constrained by accelerator mass spectrometry ^{14}C dating. Historical accounts of earthquake damage in the study region suggest that several earthquakes exposed in the trenches markedly differ in magnitude. With the exception of the most recent M~8 earthquake that occurred in A.D. 1920, two earlier events, which occurred in A.D. 1760 (or 1709) and 1638, respectively, are considerably smaller, with magnitude $M < 7$ and more likely M~6 or less. Thus, this section of the Haiyuan Fault that broke during moderate-magnitude events failed again after a short interval during a large M_w 7.8–8.3 earthquake, as part of a larger multisegment rupture. Our study shows that moderate-magnitude events can be preserved in the stratigraphy and exposed by paleoseismic trenching under ideal conditions, for instance, if sedimentation is fast enough and there is no hiatus in deposition. Eventually, the data presented add to the growing body of paleoseismic records containing events of different magnitudes with a large variability in rupture length and coseismic slip.

1. Introduction

Determining the age and size of repeating earthquakes is essential for understanding the behavior of fault ruptures and associated seismic hazard. Historical records in most regions are short compared with the repeat time of moderate to large earthquakes. Therefore, an important part of assessing the time and size of future earthquakes is to retrieve earthquake recurrence patterns from paleoseismic studies. Paleoseismology provides fundamental data for generalizing earthquake recurrence models [e.g., *Schwartz and Coppersmith*, 1984; *Sieh*, 1996; *Weldon et al*., 2004; *Berryman et al*., 2012], as well as for constraining seismic hazard assessment and forecasts [e.g., *Nishenko and Buland*, 1987; *Working Group on California Earthquake Probabilities*, 1995, 2003; *Romeo*, 2005; *Field et al*., 2014].

Paleoseismic trenching has been effective in recovering earthquake time series, yet it is notoriously difficult to determine the magnitude of paleoearthquakes. Classically, paleoseismic events are recognized in trenches based on the fact that a set of faults disrupt a suite of sedimentary layers at a horizon corresponding to the ancient ground surface [e.g., *Sieh*, 1978a; *Weldon et al*., 2002; *McCalpin*, 2009]. Stratigraphy thus provides a "temporal scale" to separate paleoearthquakes through dating of layers to constrain the timing of events. While it is sometimes possible to locally measure the size of paleoearthquake slip through careful examination of the stratigraphy, it often remains difficult, especially for strike-slip ruptures. Limited examples [*Weldon et al*., 2004; *Liu-Zeng et al*., 2006; *Kondo et al*., 2010] suffer from the ambiguity of separating the effect of single versus multiple events [e.g., *Grant-Ludwig et al*., 2010], a similar situation faced by the approach of using geomorphic offset markers [e.g., *Sieh*, 1978b; *McGill and Sieh*, 1991; *Zielke et al*., 2010; *Klinger et al*., 2011].

Events exposed in trenches are considered as surface-rupturing events, i.e., large enough to break the paleoground surface, often referred to as the event horizon [e.g., *Sieh*, 1978a; *McCalpin*, 2009; *Yeats et al*., 1997].

But the definition of surface-rupturing events in terms of magnitude equivalence is vague and often implied to be magnitude 6.5 or larger [e.g., *McCalpin*, 2009; *Akciz et al*., 2010]. This assumption is partly based on a theoretical estimate of rupture dimension on a vertical fault; in that, a *M*~6.5 earthquake is likely to fully rupture the width (<20 km) of the seismogenic layer and thus reach up to the ground surface [e.g., *Scholz*, 1982]. It is more or less consistent with observations from historical earthquakes, which show that the chance of surface rupture is less than ~50% for earthquakes of $M_w < 6.5$ [*Wells and Coppersmith*, 1993; *Weldon and Biasi*, 2015]. Thus, the notion that surface-rupturing events most likely have magnitude >6.5 only reflects the higher probability of association with surface ruptures. Eventually, however, the assumption of an existing cutoff magnitude at *M* 6.5 for earthquakes producing surface ruptures needs to be thoroughly evaluated.

In this paper, we document a case where the stratigraphic record of paleoseismic events and historical accounts of earthquake shaking in the adjacent area are combined to constrain the timing of events and their magnitudes. This provides a test of the degree of variability in size of repeating paleoruptures at this single location. At the Salt Lake trench site on the Haiyuan Fault, northwest China, the high-resolution stratigraphy of rapid deposition preserves the fine details of deformation of paleoearthquakes. The study site is within a region where the historical written record of earthquake shaking dates back to 190 B.C. [*Xie and Cai*, 1983], providing a unique opportunity for mining the vast historical written and archeological records to corroborate or augment our trenching investigation of paleoseismicity, in order to better understand seismic behavior of active continental faults.

2. Seismotectonic Setting

The ~1000 km long, active, left-lateral Haiyuan Fault is a major structure in northern Tibet. Together with the Altyn Tagh, Kunlun, and Xianshui He Faults, it accommodates the eastward movement of Tibet relative to the Gobi-Ala Shan platform to the north (Figure 1 inset) [e.g., *Avouac and Tapponnier*, 1993; *Peltzer and Tapponnier*, 1988; *Tapponnier et al*., 2001]. The Haiyuan Fault branches off the Altyn Tagh Fault in the Qilian Shan mountain range and continues eastward, striking about 110°. It then veers to a 140° strike east of the Yellow River, and to an ~NS strike along the Liupan Shan, and resumes a 100° strike again before merging with the northern boundary of the Qinling Shan.

To the north of and subparallel to the Haiyuan Fault, the Zhongwei Fault splays off with a nearly east-west strike, cuts across the Yellow River, and extends for another ~300 km before veering to the south (Figure 1b). The Zhongwei Fault, sometimes called Xiang Shan-Tianjin Shan Fault, is an oblique left-lateral fault with a large reverse component. Its strike-slip rate decreases eastward from 3.5 to 0.5 mm/yr, which is accompanied by eastward increase of vertical rate from 0.5 to 0.8 mm/yr [*Zhou and Liu*, 1987; *Cai et al*., 1997; *Liu et al*., 2006; *Yin et al*., 2013]. It is the seismogenic fault of the 1709 *M* $7_{1/2}$ Zhongwei earthquake, of which mole tracks of surface rupture were observed and documented along a 53 km rupture with a maximum horizontal slip of ~7.4 m [*W. Zhang et al*., 1988; *Nie and Lin*, 1993]. Geometrically, the Zhongwei and Haiyuan Faults may belong to a single fault system, through merging at depth to form a large crustal-stacking wedge [*Gaudemer et al*., 1995].

The Haiyuan Fault is predominantly a left-lateral fault, but the total offset and Quaternary slip rate have been controversial. About 90 km of apparent left-lateral deflection of the Yellow River was considered an indication of cumulative offset of the Haiyuan Fault [*Gaudemer et al*., 1995], whereas geological mapping of Paleozoic units and their correlatives along a section of the fault ~100 km east of the Yellow River suggested a total offset of only 10.5–15.5 km [*Burchfiel et al*., 1991]. Development of pull-apart basins along the fault was used to argue for a total offset of ~60 km since 10 Ma [*Ding et al*., 2004]. The slip rate of the Haiyuan Fault may vary systematically, for instance, by decreasing eastward along the fault because of strain partitioning among multiple splays [*Gaudemer et al*., 1995; *Lasserre et al*., 2002; *Duvall and Clark*, 2010]. Even on the central and eastern sections of the Haiyuan Fault, the Quaternary slip rate estimates are 12 ± 4 mm/yr [*Lasserre et al*., 1999], 8 ± 2 mm/yr, and ~5 mm/yr or less [*P. Zhang et al*., 1988b; *Li et al*., 2009; *He et al*., 1994, 1996; *Yuan et al*., 1998; *Chen et al*., 2014]. Modern fault slip rate or strain accumulation rate derived from GPS and interferometric synthetic aperture radar suggests a lower rate of ~5–8 mm/yr [*Cavalié et al*., 2008; *Jolivet et al*., 2012].

The Haiyuan Fault is overall segmented, consisting of a few tens of kilometers long sections, commonly separated by extensional jogs, step overs, and pull-apart basins of varying widths (Figure 1b).

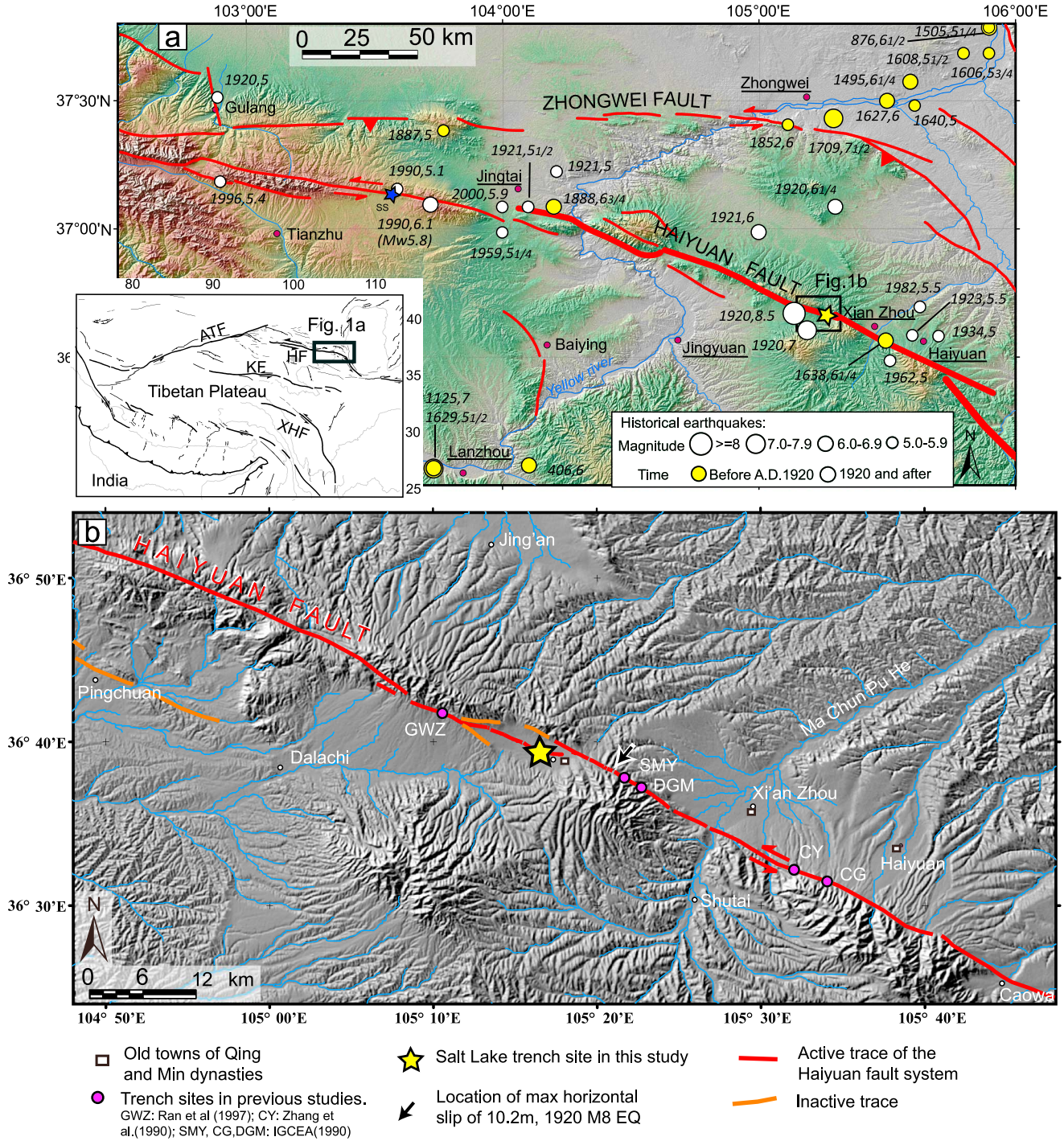

Figure 1. Seismotectonic setting of the Salt Lake trench site on the Haiyuan fault. (a) Major active faults in the region, modified from *Gaudemer et al.* [1995]. Surface rupture extent of 1920 M_W 7.8–8.3 Haiyuan earthquake is highlighted with a thick red line. Epicenters of catalogued historical earthquakes are shown as circles whose sizes are scaled with magnitude, color-coded by year of occurrence. Yellow star: Salt Lake trench site, blue star: Songshan site. Villages mentioned in historical earthquake record are underlined. Inset figure shows active faults in Tibet. (b) Shaded relief of the region in the vicinity of the Salt Lake trench site. Trench locations in previous studies are shown as filled circles. Abbreviations in inset map are ATF, Altyn Tagh Fault; HF, Haiyuan Fault; KF, Kunlun Fault; and XHF, Xianshui He Fault.

Transpressional segment boundaries are rare along the Haiyuan Fault. One of the largest extensional jogs, a 4 km wide left step, occurs at ~104°E near Jintai, at the eastern end of the great 1920 Haiyuan earthquake rupture [*LIS and NBCEA*, 1980; *Deng et al.*, 1986]. We consider this step over a boundary that separates the eastern from the western Haiyuan Fault. Immediately west of the jog, the 30 km long fault

section is creeping with a rate of ~5–8 mm/yr and relatively high microseismicity [*Cavalié et al*., 2008; *Jolivet et al*., 2012]. Trenches at ~103.5°E revealed a mixed mode of paleoseismic deformation from minor cracks of moderate-magnitude events, for instance, the 1990 *M* 5.8 Jintai-Tianzhu earthquake, to large deformation associated with large-offset events, the most recent one occurring about ~800 years ago [*Liu-Zeng et al*., 2007].

The 16 December 1920 Haiyuan earthquake of M_w 7.8–8.3 produced an ~230 km long surface rupture that crossed several geometric fault segments, with a bell-shaped slip distribution, and a maximum slip of ~10 m at the center [*Deng et al*., 1986; *Zhang et al*., 1987]. The main shock was followed a week later, on 25 December 1920, by an aftershock with magnitude ~7, whose epicenter was estimated to be ~50 km to the east of the main shock [*LIS and NBCEA*, 1980]. These devastating earthquakes inflicted 230,000–270,000 casualties [*LIS and NBCEA*, 1980; *Liu et al*., 2003] and produced widespread landslides so dramatic that "mountains walked" [*Close and McCormick*, 1922]. It was large enough to set off the first-generation seismometers around the globe. Using these early records, *Richter* [1958] estimated a magnitude 8.5 based on surface waves, which has been the commonly accepted magnitude for the 1920 Haiyuan earthquake. *Chen and Molnar* [1977] later estimated a moment magnitude of 8.3, but acknowledged that the uncertainty can be a factor of 2, especially when assuming a 45° dipping reverse fault. These early estimates may overestimate the magnitude of the 1920 Haiyuan earthquakes [*Abe*, 1981]. Given its reported rupture length and offset (230 km and 10 m), and assuming a 15 km width (depth) and predominately strike-slip faulting on a nearly vertical fault plane, it is more likely to be a moment magnitude of 7.8, as listed on the U.S. Geological Survey website (http://earthquake.usgs.gov/earthquakes/world/events/1920_12_16.php). Given these uncertainties, the 1920 Haiyuan earthquake was roughly a M_w 7.8–8.3 and thus a dramatically large earthquake.

The return time of such 1920-type earthquake multisegment rupture is still unclear. Paleoseismic investigations have been carried out on various points along the fault [*Zhang et al*., 1988a, Figure 1b; *IGCEA and NBCEA*, 1990; *Ran et al.,* 1997; *Min et al*., 2001; *Zhang et al*., 2003]. However, earlier works suffer from considerable uncertainties: (1) they rarely yield a sequence of more than three events at a single site; (2) they lack well-preserved stratigraphy to separate event horizons, and therefore, event evidence is highly interpretive; and (3) event timing was based on old, non-AMS (accelerator mass spectrometer) ^{14}C dating.

3. Site Location and Geomorphology

To better constrain the timing of past earthquakes on the eastern Haiyuan Fault, we choose to open trenches at the Salt Lake site, where the depositional environment is optimal for preserving past earthquake deformation. The site is located within the rhomb-shaped Salt Lake basin, 4 km wide by 7–8 km long, and 50 km west of Haiyuan town (Figure 1b). It is a closed basin, with short drainages of ephemeral channels collecting sediments from the surrounding hills. More than 500 m deep, the basin is filled with Quaternary sediments, nearly up to its rim [*IGCEA and NBCEA*, 1990]. Historically, the lake has been an important salt mine, since at least the Ming dynasty (annals of Haicheng County).

Bedrock in the vicinity of the Salt Lake basin consists of Precambrian gray quartz schist and marble, which outcrop on the hills to the northwest and southeast sides of the basin. Oligocene purple sandstone and siltstone outcrop at the northeast corner (Figure 2). Sediments sourced from gray quartz schist versus the red beds provide strong color contrast. Being part of the Loess Plateau (roughly 34–40°N, 103–114°E), loess is common and extensive throughout the region, mantling the lower portion of the hills around the basin (mapped as late Pleistocene in Figure 2). Southwest of the basin, a fan-shaped Quaternary conglomerate, with clast imbrication suggesting a source from the northeast, has been left laterally offset from its source by the Haiyuan Fault [*IGCEA and NBCEA*, 1990; *Burchfiel et al*., 1991].

Formation of the Salt Lake basin is controlled by the activity of the Haiyuan Fault, and although its age is not well studied, it is estimated to be Quaternary [*Zhang et al*., 1989; *IGCEA and NBCEA*, 1990; *Burchfiel et al*., 1991; *Ding et al*., 2004]. The basin is bounded on the north, southwest, and southeast sides by faults, which have a large normal component; thus, the basin has been interpreted as a pull-apart basin between N60 and 65 W striking fault segments [*Burchfiel et al*., 1991; *Zhang et al*., 1989].

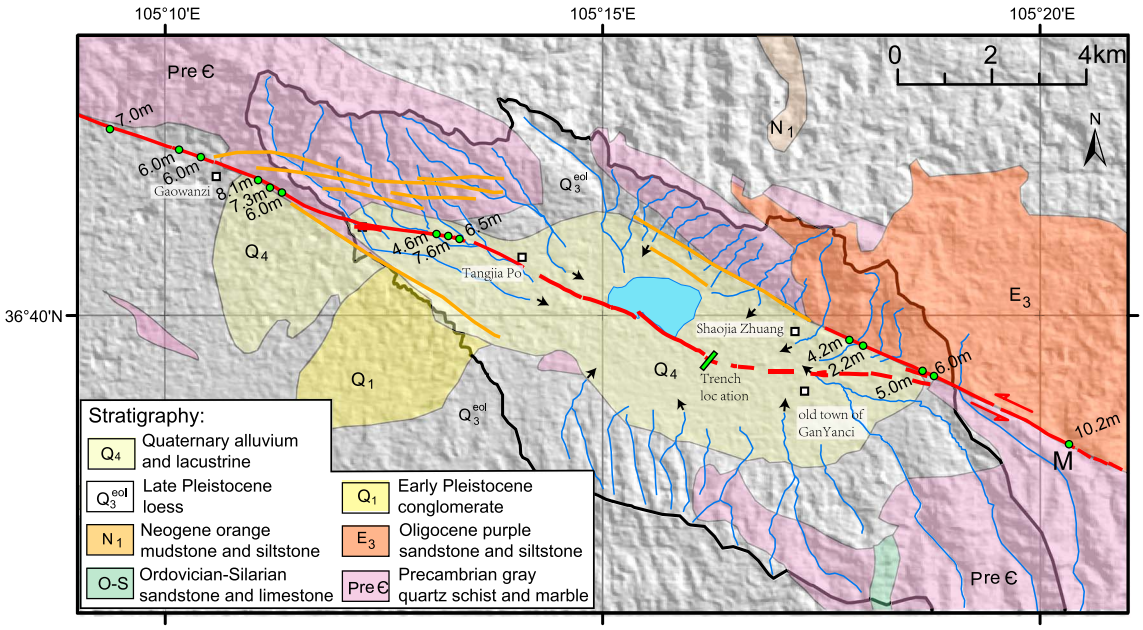

Figure 2. Geological map of the internally draining Salt Lake basin, superimposed on shaded relief of Advanced Spaceborne Thermal Emission and Reflection Radiometer digital elevation model (DEM). Fault traces that broke in 1920 are shown in red, and others in orange. Blue lines: ephemeral rivers draining to the basin; black lines: drainage divide; blue polygon: current lake extent; blue bar: trench location; green dots with numbers are coseismic left-lateral slip during the 1920 Haiyuan earthquake, where *M* denotes location of ~10 m [*Zhang et al.*, 1987].

The basin is now shortcut by a throughgoing fault, running diagonally across the basin, which produced a 2 m high north facing coseismic scarp during the 1920 earthquake [*Deng et al.*, 1986; *Zhang et al.*, 1987] (Figure 3). Due to the coseismic uplift on the southern side, the center of the lake shifted about 500 m to the north [*IGCEA and NBCEA*, 1990]. As illuminated by airborne lidar acquired in the winter of 2011, this fault scarp cuts sharply through the middle of the basin with varying heights along strike. It is most prominent in the middle of the basin, diminishing toward the east, first into a 20 m wavelength broad monoclinal scarp, then to gentle warping, and eventually disappearing before reaching the southeastern basin edge. Due to the flatness of the basin floor, markers for coseismic horizontal slip during the 1920 Haiyuan earthquake are lacking in the basin, except along the northwestern slope, where the village of Tangjiapo is located. Here a series of stone-piled farming terrace divides, possibly built sometime in Qing dynasty (200–300 years ago), were offset 6–8 m [*Zhang et al.*, 1987]. In addition, ~5 km to the east of our trench site, deflected channels indicate left-lateral offsets of 7–10 m, with one site ~10.2 m, which was considered the maximum for this earthquake [*Deng et al.*, 1986; *Zhang et al.*, 1987].

Our trench site is located ~1.5 km east of the currently active lake shoreline. The trench is thus in the peripheral region of the lake and the transitional zone between two alluvial fans, collecting sediment sourced from the north and east. At this site, the 1920 scarp is 2 m high and consists of two to three strands (Figure 3).

4. Excavations and Stratigraphy

We opened multiple fault-perpendicular trenches across the north facing fault scarp. The first excavation was conducted in 2007, producing a 40 m long 3–4 m deep trench. We cleaned the walls, which were photographed on 1 m × 1 m grid. We then mapped the stratigraphy and faults in the field on photo printouts. After mapping, we expanded the trench, by digging ~1 m sideways into the walls in the vicinity of the main fault zones and secondary branches, to gather additional evidence about events. We reexcavated at almost the same location in 2009, making it wider and deeper, so that for each fault strand, we have a total of six trench exposures, labeled as T09W, T07WW, T07W, T07E, T07EE, and T09E, respectively, from west to east. Multiple exposures display lateral variation in deformation style for each event along strike.

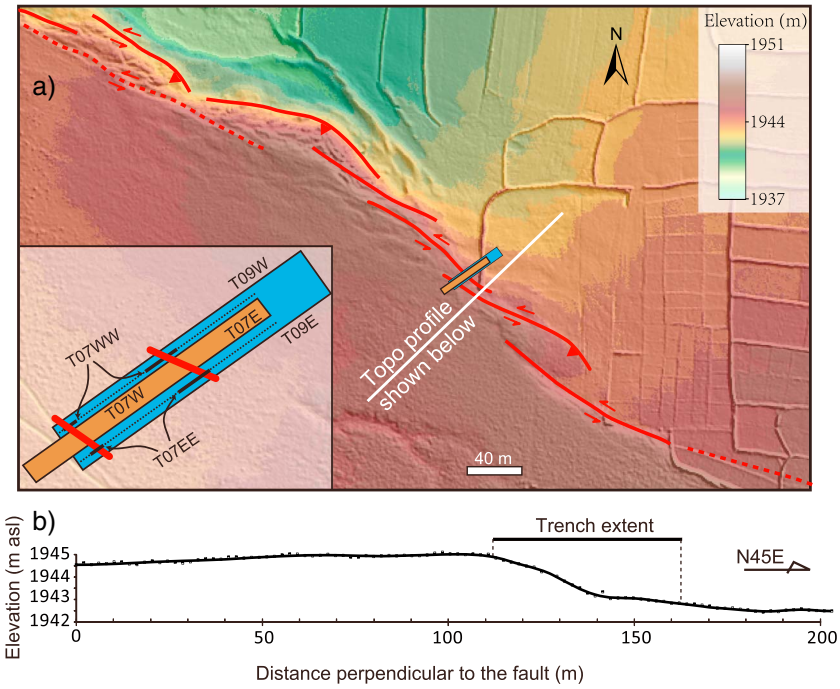

Figure 3. Map of trench site showing (a) fault zone geometry and trench location. Note the en echelon nature of fault zone and right stepping fault strands. Base map is 0.5 m resolution lidar DEM superimposed on shaded relief, collected in 2011, 5 years after the first trenching season. Inset map shows configuration of 2007 and 2009 trenches and exposure naming scheme. (b) Fault perpendicular topographic profile near trench site. Our trenches cover the main portion of the 2 m high north facing scarp.

The trenches exposed excellent stratigraphy at the site, consisting of thinly bedded alternating layers of different grain sizes and colors, due to fast deposition rate and contrasting sediments from different sources (Figure 4 and Table 1). The sediments are generally fine in grain size, comprising mostly of a combination of sand, silt, and clay, suggesting a relatively low-energy depositional facies, in accord with the distal fan-lacustrine setting. Gravelly pebbles and coarser clasts are rare in the trenches, appearing only locally in small and shallow channels, trending oblique to trench walls. Major units have constant thickness and are laterally continuous, and thus, it is fairly straightforward to correlate units from trench to trench and across the fault zones.

Figure 4 shows a composite column of 4.8 m thick exposed stratigraphy. The sedimentation rate changes with depth and over time. At an extreme, the deposition rate in the upper 2.7 m thick sediments reaches ~5 mm/yr, 2–3 times or higher than below. It is unclear whether this dramatic increase in sedimentation rate is a local consequence of a migrating deposition center or is a basin-wide increase resulting from increased erosion rate of the surrounding hills. The upper section (above 2.7 m depth) is the most distinctive group of strata. It is separated from the lower section by an organic-rich, dark soil horizon near ~2.7 m depth (Figure 4), which also marks a depositional hiatus. The upper section comprises rhythmic centimeter-thick interbedded layers of well-sorted sand and silt with alternating colors of pinkish red to light gray. Bioturbation is minor within the section. Each layer is well-sorted, either massive or horizontally bedded, with upward fining or coarsening deposition structures well preserved.

Consistent with a lower sedimentation rate, the deeper part of the stratigraphy (below 2.7 m depth) contains more clay-rich, thicker, and more homogeneous layers. The deposits in this lower section may represent a relatively more stable subaqueous environment, similar to a previously documented deposit of dark gray clay with few stratigraphic markers documented elsewhere [e.g., *Rockwell et al*., 1986; *Weldon et al*., 2002; *Daëron et al*., 2007; *Liu-Zeng et al*., 2007]. Layers or horizons containing dark organic matter are frequent in the deeper stratigraphy but not in the upper 2.7 m. These layers represent periods of nondeposition and soil formation [*Weldon et al*., 2002].

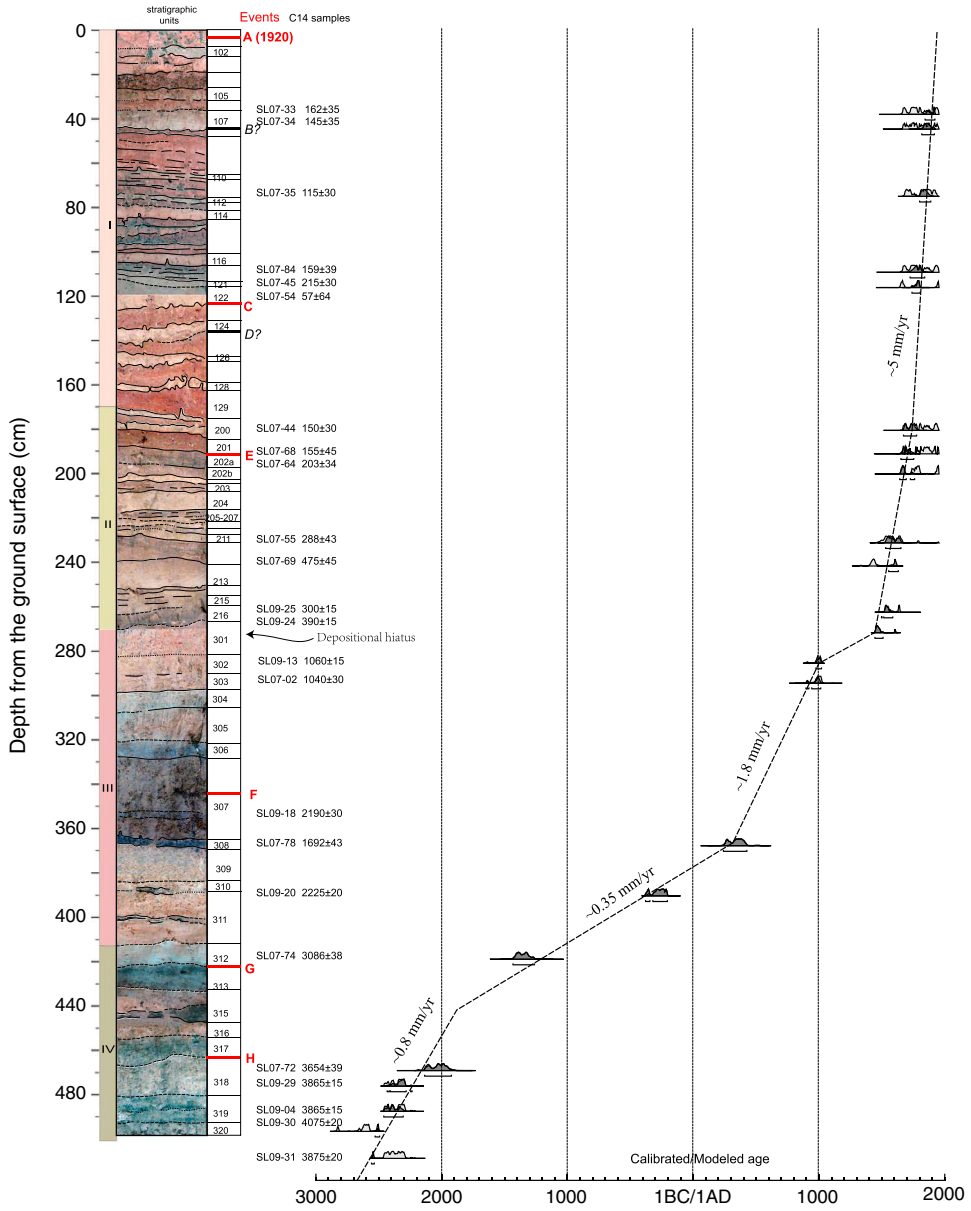

Figure 4. Composite stratigraphic column of units based on photo mosaic of trench exposures of representative stratigraphy at the Salt Lake site. Unit contacts are shown as black lines. Interpreted event horizons for A through J are shown in letters. Red letter in bold denotes probable event, italized and question marks for those possible to unlikely events. Detrital charcoal samples returned radiocarbon (^{14}C) ages that were mostly in correct stratigraphic order. Radiocarbon ages were calibrated and statistically analyzed using Oxcal 4.2, and atmospheric data from *Reimer et al.* [2009]. Calibrated 14C ages are shown on the right side.

5. Paleoseismic Evidence of Events

In this section, we focus on presenting and discussing paleoseismic events preserved in the upper 2.7 m thick section of the stratigraphy, because fine details of deformation are well preserved in this package of the high-resolution stratigraphy.

In our trenches, the main fault zone consists of multistranded, 60° south dipping faults, which intersect with the ground surface at the base of a 2 m high geomorphic fault scarp. The fault shows a reverse sense of dip-slip motion, with left-lateral strike slip, making it overall transpressional, even though the general structural setting is a shortcut through a pull-apart basin. The reverse component is a local, secondary effect of fault dip angle and a transpressional step associated with en echelon arrangement of strike-slip fault traces

Table 1. Summary of Stratigraphy Exposed in the Salt Lake Trenches

Grouping	Unit Number	Descriptions and Notes
USL-1 (I)	101–107	Alternating layers of reddish massive bioturbated sand and silt (101, 103–104, and 106) and relatively well sorted gray medium to fine sand (102, 105, and 107). 105: a distinctive layer with relatively well sorted, homogeneous gray fine sand and silt, which is continuous and with uniform thickness, correlative among trench exposures. Bioturbated but still visible of slightly upward coarsening structure. 107: a distinctive layer of massive light gray upward fining unit of medium to fine sand to silty very fine sand.
	108–109	Occurring only locally, reddish homogeneous sand and silt.
	110 and 112	Massive pinkish fine sand to silt.
	111	An approximately millimeter-thick layer of well-sorted gray very fine sand to silt.
	113 and 115	A succession of rhythmic sediment. Lens-shaped, developed only in sags near the fault zone, pinching out within ~2 m on two sides. Medium sand with well-preserved sublayer stratigraphy and beddings.
	114 and 116	Distinctive layers of relatively well-sorted pinkish gray silt and very fine sand, which can be traced in all exposures.
	117–120	Pinkish to brownish red homogeneous massive sand and silt, occurring locally in sags, with thickness pinching out quickly.
	122	A distinctive and continuous layer of light gray massive silty fine sand, of slightly varying thickness but stable occurrence across all exposures.
	123–128	A package of alternating layers of reddish to brownish massive fine sand (123, 125, and 127) and gray to light gray massive silty fine sand (124 and 126). Variable thickness but can be continuously traced in all exposures, with wavy contacts between units, thickness suggesting interfingering aggradation.
	129	Prominent layer of red to dark red medium to fine sand, locally coarse sand, of varying thickness.
USL-2 (II)	200a–200c	Distinctive lens-shaped layer, thickest near the fault zone, pinched out 7–8 m south of the fault, with prominent erosion (scouring) lower contact with unit 201. 200a: light gray silt with sharp lower contact. 200b: light reddish gray silty fine sand. 200c: light gray silt, with sharp lower contact.
	201	A generally upward coarsening layer of pinkish clayey silt for the bulk part, to fine sand to medium sand, the color becomes darker upward, with dark red fine sand of variable thickness at the very top.
	202	202a: dark gray silty clay, with laminae of dark brown clay strings at some places. 202b: an upward fining sequence from gray fine sand to gray with red taint sandy silt.
	203	Pale red very fine sand to silt, gradational contact with unit 204.
	204	White to pinkish white fine to silty very fine sand, with many minute fragments of charcoal. Variable layer thickness, with scouring lower contact at some places. At places of greatest thickness, consists of two sublayers of upward coarsening sequence for each.
	205	A distinctive bed of relatively well-sorted light brown medium to fine sand, with nearly stable thickness. Consists of two sublayers of same color but slightly coarser in the lower one.
	206	2–6 cm thick white to pinkish white well-sorted very fine sand, locally with upward fining structure.
	207	Similar to unit 205, it is a distinctive layer of light brown medium to fine sand, with stable thickness. Consists of two sublayers: the lower one of medium to fine sand, with upward fining structure, and sharp scouring lower contact, the upper one very fine sand.
	210	A distinctive reference layer, with stable thickness ~3 cm, of white to pinkish white fine sand to silt, with upward fining structure. The lower contact is defined by a peat-like string and locally sharp.
	211	Consists of two sublayers: the lower one is white to light gray silt to very fine sand; the upper one of darker in color, with alternating laminae of pink red fine sand and dark brown peat-like strings.
	212	Package of alternating 2–3 mm thick gray and pink red lamiae of silty fine sand, with discontinuous dark/dark brown peat-like strings.
	213	213a: occurring only locally, lens of silt. 213b: gray with yellow taint fine sand fining upwardly to brownish clay.
	214	Pale red massive silty fine sand of varying thickness. Upward fining sequence from gray fine sand to brownish gray silty fine sand.
	215	A distinctive reference layer of light grayish medium sand, with relatively stable thickness of ~7 cm. Recognizable upward coarsening structure from fine sand to medium sand, the top locally containing a thin layer of ~1 cm light gray silt.
	216a	Light brownish gray silt, with the top grading into gray clayey silt.
	216b	Dark brown clay with a couple of discontinuous peat string horizons. The color deepens downsection. The lower contact with unit 301 is gradual, but in some location, it is a dark peat-like horizon.
MSL-1 (III)	301–307	301–307 is a package of massive brownish red to light brownish clay to silty clay (302, 305, and 307), separated by thin layers of dark brown clay (301, 303–304, and 306). 301 is brownish red clay. 302 is brown to dark beige silt, in places brick red color in the lower 20–30 cm, and the bottom consisting a discontinuous thin layer of red clay.
	308	Distinctive thin (approximately centimeter thick) peat-like layer. Clear and continuous to act as deformation marker layer.
	309	Homogeneous massive brownish clay.
	310	Overall gray to light gray sandy clay, with discontinuous dark peat-like layers.

Table 1. (continued)

Grouping	Unit Number	Descriptions and Notes
	311	Light brownish sandy clay.
MSL-2 (IV)	312	Light greenish gray very fine sand to silt.
	313	Light brownish clay. Lens-shaped, thickest near the fault zone.
	314	Light red clayey sand. In units 314–320, carbonate concretions are ubiquitous.
	315	Gray to dark gray clay. The lower boundary is marked by a thin brown clayey layer.
	316	Light red silty clay, with whitish carbonate precipitation granules.
	317	Gray to dark gray
	318	Light greenish gray clayey fine sand, the upper part gray to dark gray and lower part relatively lighter in color and coarse in grain size.
	319	Overall dark gray clayey sand, containing black peat-like sublayers with many charcoal fragments.
	320	Wedge-shaped yellowish green massive well-sorted fine sand.
LSL (V)	400	Light gray to white sandy silt and clay. Indurate, with blobs of white calcareous concretions.
	401	Yellowish brown clayey fine sand, the top part containing light gray to gray clay.
	402	Light red clay, massive, the upper part locally lighter in color.
	403	White to light gray clay.
	404	A mottle-colored mixture of yellowish brown and light gray fine sand. The lower ~5 cm is more brownish in color than that above. Units 401–404 are folded, in a convoluted way.
	405	Pale green clayey very fine sand to silt, with yellow and dark spots, probably due to biogenic processes. Both contacts with units above and below are gradational.
	406	Red to husky red, massive but heterogeneous, very fine sand to clay. The top portion containing horizons of medium to find sand. The base of the unit was not exposed.

(Figure 3a). The stratigraphy on the hanging wall is tilted, more or less parallel to the slope of the current ground surface. A secondary fault zone consisting of nearly vertical and forked fault strands occurs at 7–9 m south of the main fault and on the hanging wall (Figure 5). In some exposures, the secondary fault shows a normal sense of vertical component, where the fault dips to the north toward the main fault zone.

Three and possibly four paleoseismic events are preserved within the upper section, named in letters (Figure 4). Evidence for individual events varies in robustness. Stratigraphic evidence of paleoseismic events and the likelihood of event horizons are evaluated using the scheme of *Scharer et al*. [2007]. Events A, C, and E most probably correspond to surface-rupturing events. They are supported by strong evidence unambiguously interpreted as coseismic deformation. By comparison, the indicators for events B and D are either nonunique or too ambiguous in the stratigraphy to be undoubtedly associated to distinct events. As shown later, ambiguity in the veracity of these event horizons is mainly due to the upward termination of brittle faulting cracks at levels slightly below the event horizon, i.e., not breaking to the surface.

5.1. Most Recent Event A (the 1920 Haiyuan Earthquake)

The most recent ground-rupturing event **A** relates to the 1920 Haiyuan earthquake. Evidence for event A is clear and strong in all six exposures. This event produced mole-track-like push-up mounds above south dipping faults, and caused tilting of strata on the hanging wall, on the order of 4–6° (Figures 5–8). The long-wavelength tilting shown in exposures corresponds to the fault scarp seen on the surface. Degradation of the scarp is indicated in the stratigraphy, as a wedge of colluvium on top of dipping faults, and a small amount of erosion of the top layers on the hanging wall (Figure 5a). This is mostly clear in exposure T09W, where flattening of fault dip near the surface resulted in overthrusting of unit 102 and the collapse of the hanging wall to form a wedge of colluvium (Figure 5a).

Expression of event A on the secondary strand is shown only in wall T07WW, in the form of open fissures widening upward to the surface, with blocks of surrounding rock collapsed inside (Figure 6e). In other exposures, this event is unclear, possibly because opening of fissures are too small to be noticed.

The main fault zone is typically multiple-stranded, consisting of two or more intertwining fault strands, with rotated blocks in between or blocks falling into fissures (Figures 6a, 6c, 7a, and 7b). Tilting and long-wavelength folding of the hanging wall strata must have accommodated a considerable amount of vertical

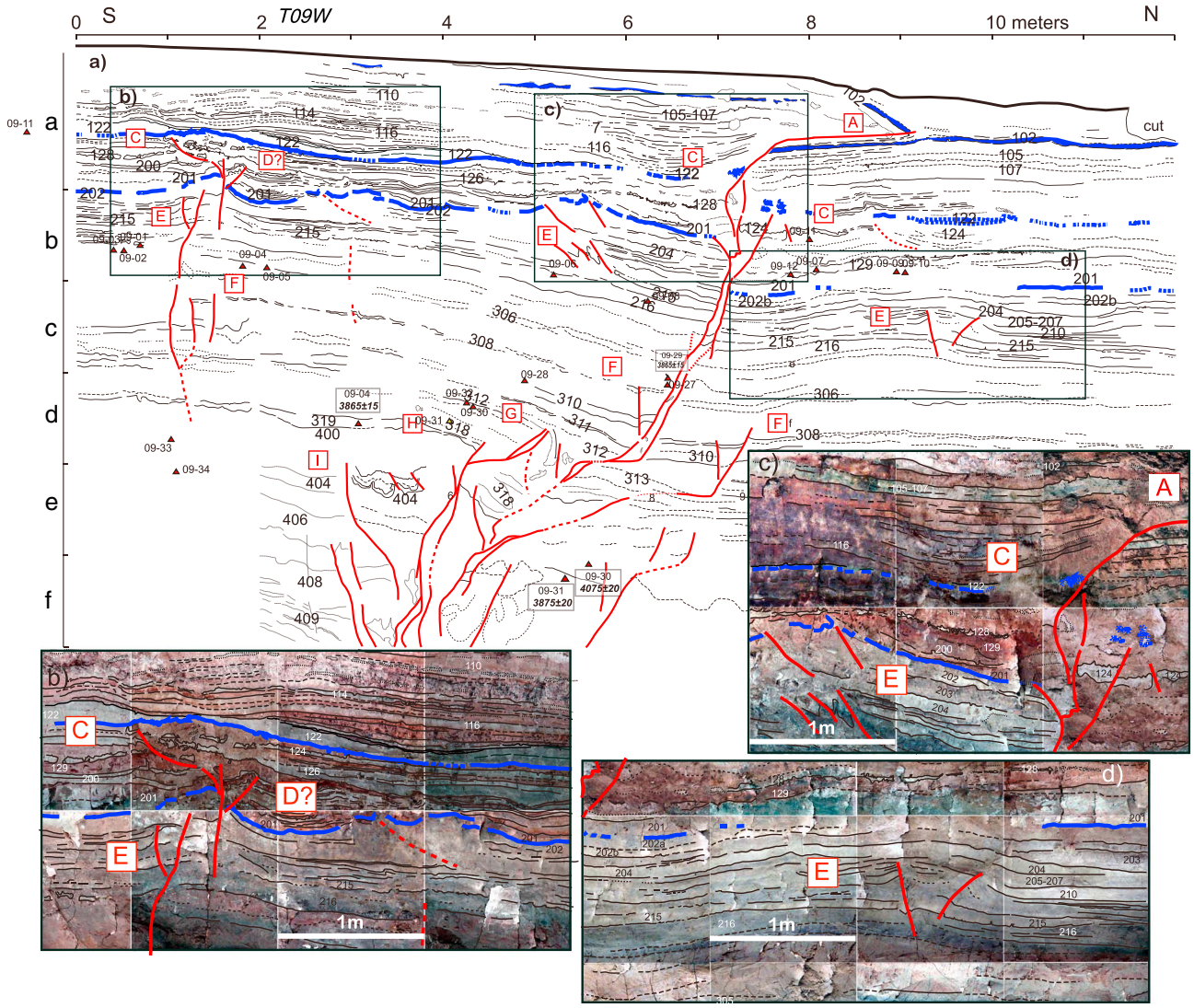

Figure 5. Trench logs showing stratigraphy and faults in exposure T09W. (a) Overall mapping of sketched lines. (b–d) Mapping of enlarged portions with critical evidence of events, superimposed on mosaiced photos. Locations are indicated in Figure 5a. One-meter grid is shown by number in horizontal (starting 0 from the south and increasing toward the north) and alphabet in vertical (a through f from top to bottom). Trench wall flipped to show north to the right. Stratigraphic units are labeled numerically; interpreted event horizons by capital letters, and question marked when uncertain. Event horizons of C and E are traced by thick blue lines. Sample locations are denoted by triangles, with calibrated ^{14}C age and 1σ range shown.

deformation, making the 1.5–2 m high monoclinal scarp. In contrast, the apparent brittle vertical offset across the main fault zone is small, mostly 20–40 cm, and only up to ~50 cm in exposures T07W and T07WW, where the main fault zone narrows and thus deformation is more localized.

5.2. Penultimate Event C

The penultimate event **C** occurred when unit 122 or 123 was at, or near, the ground surface. Some of the most compelling observations for event C are exposed in wall T09E at the position of 1 m (Figures 8a and 8b). There, two north dipping normal faults separated from the main fault zone offset units 122 through 300, producing an ~20 cm high scarp, with vertical offset and tilting of strata against flat-lying layers across the fault. The highest level at which the fault can be traced is unit 122. Deformation is also manifested by a synclinal warp formed in the hanging wall, which was subsequently filled by a lens-shaped package of alternating layers of laminated and well-sorted sand and silt of units 110–122 (2–5 m in Figures 8a and 8b). This line of evidence for event C on the secondary fault branch is shown in all exposures, slightly different

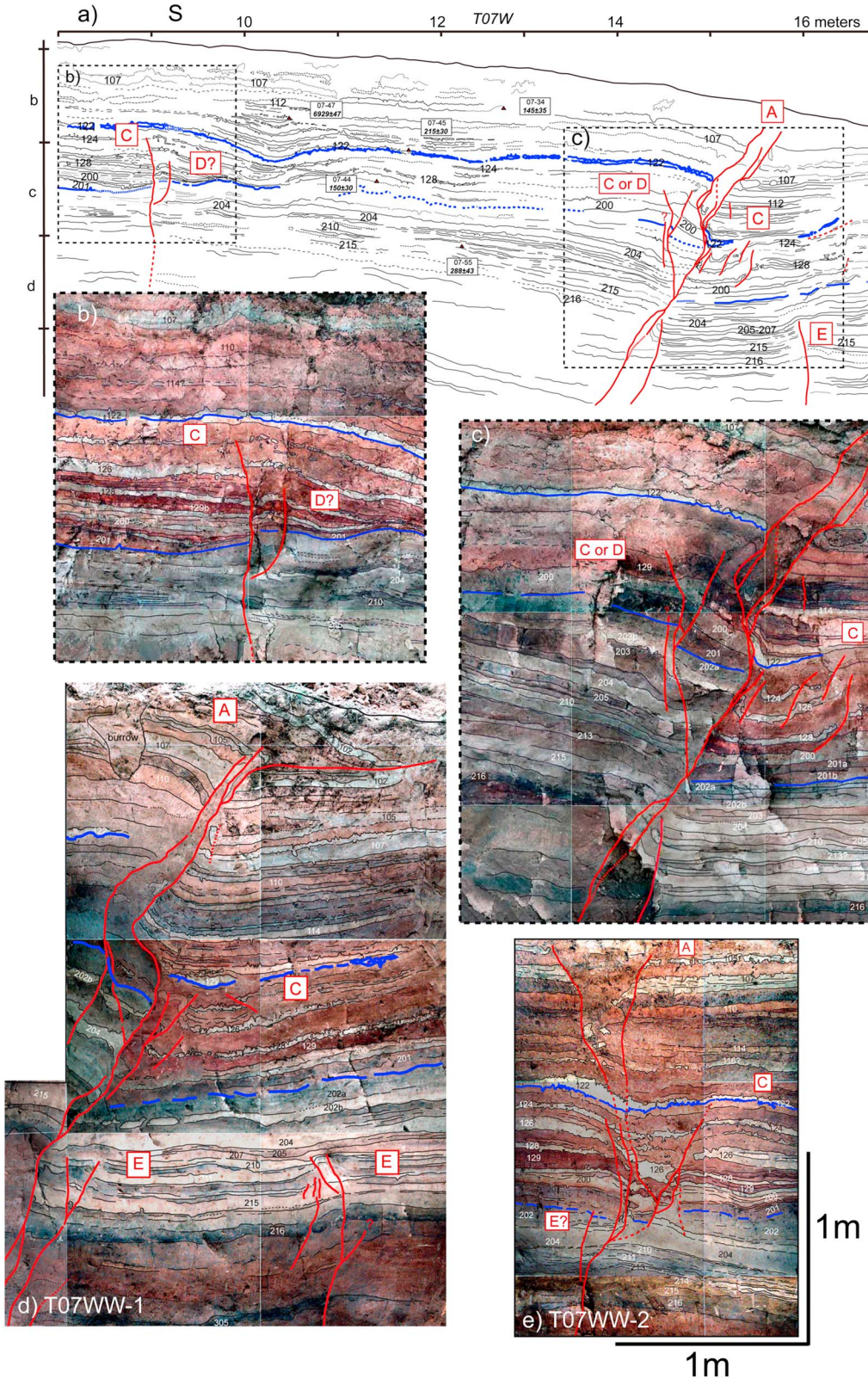

Figure 6. Trench logs showing stratigraphy and faults in exposures T07W and T07WW. (a) Overall mapping of sketched lines. Event horizons of C and E are traced by thick blue lines. (b and c) Mapping of enlarged portions of exposure T07W with critical evidence of events, superimposed on mosaiced photos. Locations are indicated in Figure 6a. (d and e) The enlarged portions in exposures T07WW, corresponding to 14–16 m (near the main fault zone) and 8–9.5 m (the secondary branch), respectively. See Figure 5 for descriptions of grid and symbols.

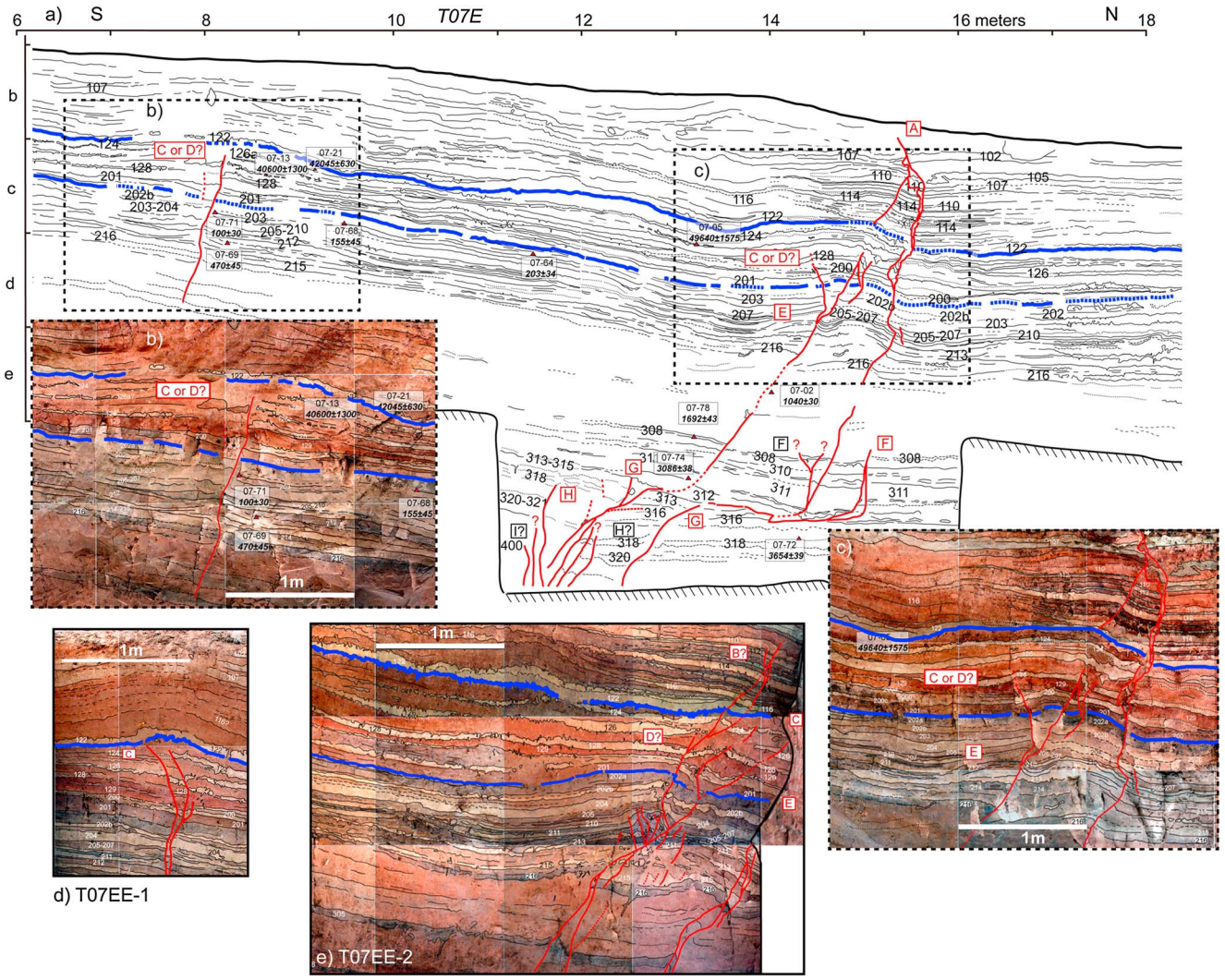

Figure 7. Trench logs showing stratigraphy and faults in exposures T07E and T07EE. (a) Overall mapping of sketched lines. Event horizons of C and E are traced by thick blue lines. (b and c) Mapping of enlarged portions of exposure T07E with critical evidence of events, superimposed on mosaiced photos. Locations are indicated in Figure 7a. (d and e) The enlarged portions in exposures T07EE, corresponding to 8.5–10 m (the secondary branch) and 13.5–17.5 m (near the main fault zone), respectively. Locations of fault traces shift slightly between exposures due to the obliquity between trench exposures and fault strike. See Figure 5 for descriptions of grid and symbols.

in brittle offset depending on fault dip angle but similar in synclinal warping and overlying lens-shaped growth strata on top (Figures 5b, 6b, 7b, 7d, and 8b).

In the main fault zone, the pattern of deformation associated with event C changes along strike. In exposure T09W (Figure 5c), it is shown as a colluvial wedge below the lens-shaped package of units 110–116. Toward the east, it is in the form of syncline in exposures T07W and T07WW (Figures 6c and 6d), then a broad pop-up warp above a south dipping branching fault tips in exposures T07E and T07EE (Figures 7c and 7e). In exposure T09E, it changes to slightly tighter amplitude, with flower-type upwarping of units 124–129 (Figure 8c).

5.3. Third Youngest Probable Event E

Event E is stratigraphically separated from event C, with the event horizon lying between units 201 and 204, and most likely near unit 202. Despite some uncertainties in the exact event horizon, evidence for event E is remarkably clear, persistently shown in all exposures as folding of units 203–205 above dipping faults.

Fold geometry varies sharply along strike, changing from anticline to monoclinal step, then to a paired anticline and syncline, and then to an anticline again in successive exposures (Figures 5–8). The most

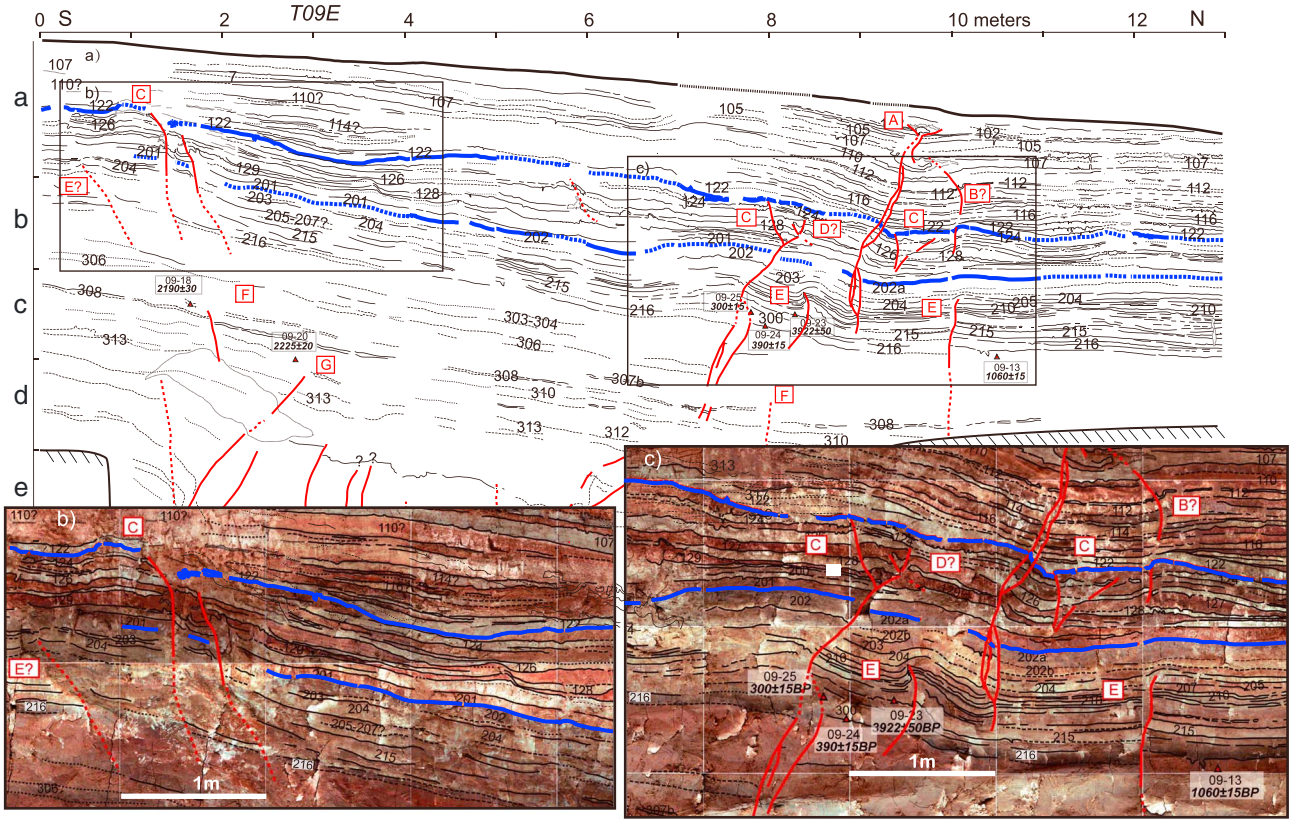

Figure 8. Trench logs showing stratigraphy and faults in exposure T09E. (a) Overall mapping of sketched lines. (b–d) Mapping of enlarged portions with critical evidence of events, superimposed on mosaiced photos. Locations are indicated in Figure 8a. See Figure 5 for descriptions of grid and symbols.

representative evidence for event E is in exposure T07EE (Figure 7e). Here thinly bedded stratigraphy clearly preserves deformation of a flower-like push-up above the south dipping fault, forming an anticline and subsidiary syncline. Units 215–205 are convoluted and more intensely deformed than the overlying units 204–202, suggesting a degree of decoupling and an angular unconformity. In exposure T09E (Figure 8c), event C is clearly exhibited as a paired syncline and anticline of 1 m wide in wavelength, with a pointed fold crest affecting units up to 205. Units above (204–202b) are also warped but with decreasing amplitude. A subvertical lone fault with sharp offset provides additional evidence for this event in this exposure. The amount of apparent vertical separation decreases upsection; the brittle fault turns into warping of diminishing amplitude upsection.

Considering the suite of deformation level in all exposures, the youngest units affected by event E are 202–203. We thus interpret that unit 202 was at or near the ground surface at the time of faulting and folding. As shown in exposure T07EE (Figure 7e), the wedge-shaped unit 201 thins toward the top of the anticline, resembling growth strata and filling of a topographic low in the synclinal trough. In exposure T09W, complete disturbance of the stratigraphy, indicated by homogenized strata with original sedimentation structures erased, occurs locally across a 4 m wide section of the wall (Figures 5a and 5d). It only affects a sediment package of limited thickness, units 202–215, below which the stratigraphy is undisturbed. This resembles shaking-related soft-sediment deformation [*Allen*, 1986; *Marco et al*., 1996]. An angular unconformity appears as a wavy unit boundary between disturbed package and overlying units 201–129, which are lens-shaped in thickness so as to fill in depressions, and capped by the flat-lying unit 128.

It is common in our trenches that faulting and warping associated with event E stop slightly below the event horizon, unit 202. For instance, in T07WW wall (Figure 7d), brittle faulting diminishing into a ripple-like scarp stops at unit 205, which is capped by the overlying undisturbed unit 204. Similarly in wall T09E (Figure 8c), two brittle faults turn upward into folds, which diminish gradually and disappear within 202b–203, centimeters below the interpreted event horizon. This pattern indicates that upward fault termination can

Journal of Geophysical Research: Solid Earth

10.1002/2015JB012163

Table 2. Table Summarizing Evidences for Each Event at the Salt Lake Site[a]

Event	Trench wall	Location (m)	Type of Evidence	Youngest Unit Affected	Oldest Unit Undisturbed	Descriptions and Rating of Evidence
A	T09E	9–10	tb, mt, and vo	102	Ground surface	Flower-type push-up mount of unit 102 (mole track?), hanging wall tilting of entire stratigraphic package. Wedge-shaped scarp colluvium and angular unconformity of postevent deposit covering the toe of scarp colluvium (**S**).
	T07E	16–17	vo and fis	102	surface	Linked multistranded fault zone. A block of unit 107 falling into a fissure, ~30 cm appearance vertical offset of unit 107 across the fault zone. Titling of beds to the north of the hanging wall above a south dipping fault (**S**).
	T07W	14–15	vo and fz	102	surface	Complex multistranded intervening fault zone with unit 107 being offset ~20 cm, blocks of offset units rotated between fault strands (**S**).
	T07WW	~14	au, cw, tb, and vo	102	surface	Sharp offset of near-ground surface units 107 through 102. Shearing on south dipping fault causes dragging of units on the hanging wall. Flattening of fault dip angle at the surface produces a wedge and doubling of unit 102 on the hanging wall to cover that on the footwall (**S**).
		7–8	fis and vo	105		Tensional crack with fissure fills; units 102–105 show a few centimeters apparent vertical offset (**S**).
	T09W	8–9	cw and au	102	surface	Sharp offset of near-ground surface units 107 through 102. Flattening of fault dip angle at the surface produces a wedge and doubling of unit 102 on the hanging wall to cover that on the footwall (**S**).
B	T09E	10–11	vo and ut	107 base	106	Upward branching of two strands. One strand extends into unit 107; warping of units above suggests that it could be a soft link with and jump to a strand ~50 cm to the south in the main fault zone and thus breaking to the surface (event A) (**W**).
				110 base	107 base	Sharp offset of units 129–110 with vertical separation of ~7 cm. This strand is characterized as upward termination and offset decreases in amount and eventually loses the trace (dashed in the trench log) (**M**).
	T07EE	17–18	vo and ut	110 base	109	Two traces branch upward with vertical offset diminishing, with one disappearing within unit 109, the other one within 110 (**M**).
C	T09E	1–2	vo and tc	124	110	Units 126–122 are flat-lying on the southern side of the fault, and north dipping on the northern side. Apparent vertical offset is ~25 cm. Evidence for an event is compelling but could be ambiguous in event horizon, either above unit 122 or above 124 (**F** or **M**).
		8	ut and vo	125	122	Vertical offset can be traced into unit 126 and then diminishes to negligible in unit 124 (**M**).
		9–10	vt and tc	123	117	Push-up between two branches, with one branch offsetting stratigraphy up to the base of 122, and dying out within unit 122, the other trace of diminishing offset to nearly zero within unit 123. Both merge and disappear downward, i.e., rootless fault (**S**).
	T07EE	9–10	vt, au, and mt	122	116	Two faults cuts through unit 124, and the overlying unit 122 shows warping above fault. Evidence for faulting is clear yet event horizon can be ambiguous. Overlying units show a broader anticlinal warping, possibly due to effects of younger events (**M**).
		16–17	vt	124	116	Fault offset thin-layered unit 124 and capped by 116. Unit 122 pinches out in the fault zone (**M**).
	T07E	8–9	ut	128	122	Offset of 128 across the fault strand is clear; however, the level of its upward termination is not well preserved and the corresponding event could equally be C or D (**M**).
	T07W	~8	vo	126	122?	Sharp offset of 126 by ~5 cm, apparent vertical offset diminishes. Unit 122 is not offset but broadly warped. Overlying units fill the sag to the north of the fault and pinch out, forming an angular unconformity (**F**).
		14–15	au	124	122?	Units 128 through 123 are deformed as a rootless syncline. Evidence is strong, but whether the event horizon is below or above unit 122 is ambiguous due to overprinting of younger deformation. The lens-shaped unit 122 suggests deposition in a depression (**S**).
	T07WW	7–8	vo	124	122?	Fault strand cuts through unit 124. Bending of the unit outside the fault zone, probably due to diffuse deformation. It is ambiguous whether the faulting terminating within unit 123, or above unit 122, due to the upward diminishing in deformation and overprinting of the younger event A (**M**).
		~8	vo	126	116	Unit 126 is offset with ~10 cm downdropped toward the south; the apparent vertical offset diminishes upward rapidly, reducing to bending of unit 124 by 7 cm and disappearing below unit 122 or shortly above (**F**).
		13–14	au	124	122?	

AGU Journal of Geophysical Research: Solid Earth

10.1002/2015JB012163

Table 2. (continued)

Event	Trench wall	Location (m)	Type of Evidence	Youngest Unit Affected	Oldest Unit Undisturbed	Descriptions and Rating of Evidence
						Reverse sense of folding and faulting of units 126 through 124. The lens-shaped unit 122 suggests local deposition in depression. Units overlying 122 show up locally near the fault zone but in wider extent than 122 (**S**).
	T09W	7–8	vo	124	107	Unit 124 is offset, but the exact level of termination is poorly constrained due to poor stratigraphy (**F**).
D	T09E	8–9	tb and vo	127	124	Blocks of unit 128 being squeezed and tilted, with upward termination uncertain (**M**).
	T07EE	16–17	vo and cw	128	124	Two splays of fault, unit 128 being offset, broken pieces rotated, unit 126 shows rapid decrease in thickness near the fault zone, indicating on-lapping against a scarp (**F**).
	T07E	14–16	ut, tb, and vo	129	126	One strand branches upward, offset unit 129, and dies out within 128 or slightly above (**F**). Tilted blocks of unit 128 between two fault strands. Deformation could be overprinted by younger events (**F**).
	T07W	8–9	vo and ut	128	126	Folding and buckling of unit 128. Apparent vertical offset terminates within unit 127 (**W**).
		14–15	ut and vo	129	124?	Unit 129 is been squeezed and upwarped between fault branches. Upward termination is ambiguous due to poor or disturbed stratigraphy. Event C or D (**M**).
	T09W	1–2	ut	128	126	Two fault splays terminate below unit 126 (**W**).
E	T09E	0–1	vo and ut	204	129	Unit 204 and those below are flat south of the fault trace and tilted on the north. In the vicinity, stratigraphy is not well preserved; thus, the exact event horizon is not well constrained (**W**).
		8–9	fd and au	205	201	Folding of units with pointed tip affecting units up to 205. Units above (204–202) cover the fault tip but still resemble folding of decreasing amplitude (**S**).
		~10	au and vo	204	202	Subvertical fault with sharp offset, amount of apparent vertical separation decreases upsection, forming an approximately centimeter high south facing scarp. Units 204 and 203 drapes over the scarp and thicker on the downdropped side, filling the south facing scarp. Both fault and event horizon are well preserved (**S**).
	T07EE	16–17	mt and au	205–207	204	Flower-like push-up above a south dipping fault. Thinly bedded stratigraphy preserves very clearly deformation as a major anticline and a subsidiary syncline. Angular unconformity between 204 and underlying intensely deformed units (**S**).
	T07E	15–16	au and mt	205–207	204	A prominent syncline and paired minor anticline. The fault trace underlying the fold is reactivated and overprinted by younger events (**S**).
	T07W	~15	scarp and au	203	201	South facing monoclonal scarp overlying a fault that cuts through unit 210. Unit 205–207 draping over the scarp, thickness and grain size increasing on the downdropped side. The overlying sandy layer of unit 203 shows similar feature (**S**).
	T07WW	13	vo and au	210	204	A ripple-like scarp above a fault bounding a graben to the north, and matching south bounding fault 1.2 m to the south, across which there is a facies change (**S**).
		14–15	vo	207	202b?	Splays of forked faults. Units between fault traces pushed up (**F**).
	T09W	1–2	mt	215	203	A low bulge ~1 m in width shown by unit 300 and a smaller wavelength bump above a vertical fault. Units 203–204 pinch out against the bump as on-lapping sequence (**S**).
		2–6	au	202	126–128	Widespread shallow but strong disturbance of units 202–215, stratigraphy being convoluted and locally homogenized resembling shaking-induced soft-sediment deformation. Flat-lying unit 126 caps the deformed sediments. At location 5–6 m, the oldest undisturbed unit is 128, slightly lower than at other places (**S**).
		9–10	fd	204	202	Thin-skinned anticlinal folding and faulting that cannot be traced down lower than 300, the shallowness suggesting shallow buckling (**F**).
F	T09E	1–2	ut	308	304?	Offset of marker bed 308, northern side downdropped. The exact level of fault upward termination is not clear; unit 304 is the first unit that caps the fault (**M**).
		~8	ut	308	?	Vertical offset of unit 308 is clear, but upward termination of this strand is ambiguous and could be part of the younger event E (**W**).
	T07EE	15–16	vo	308	306	Vertical offset of marker unit 308, fault traces capped by unit 306 (**F**).

Journal of Geophysical Research: Solid Earth

10.1002/2015JB012163

Table 2. (continued)

Event	Trench wall	Location (m)	Type of Evidence	Youngest Unit Affected	Oldest Unit Undisturbed	Descriptions and Rating of Evidence
		16–17	vo	308	?	Vertical offset of unit 308, the overlying stratigraphy is not clear to constrain the upward termination (**M**).
	T07E	15–16	vo	308	306	A splay from the main fault offsets units 310–308 (**W**).
		~16	vo	308	?	Clear offset of units 310 and 308, with ~3 cm down on the southern side sense of motion (**F**).
	T07WW	13–14	vo and tb	308	306	Two fault strands offset unit 308, with a couple of cm vertical separation, causing unit 308 tilted between two fault strands (**S**).
	T09W	1–2	vo	308	302	A few centimeter offset across the fault. Directly below a fault in the younger units, thus ambiguous whether it is a segment of the fault trace in younger event (**M to W**).
		6–7	ut	308	306	An upward branch that can be traced cutting through unit 308 and caused a couple of centimeter offset; the level of upward termination is not clear (**M**).
		7–8	vo and ut	308	301	Unit 308 is offset by two branches, forming an asymmetric graben. The overlying unit 305 shows the feature of draping over a half-graben, either coincidence or indicating the upward termination of north bounding fault effect (**F**).
G	T09E	2–3	vt	313	308	Offset of unit 313, northern side uplifted. Stratigraphic level of event horizon is loosely constrained. But unit 308 is not affected; therefore, it is a separate event from event H (**M**).
	T07EE	14–15	fz, vo, and cw	314	312	Fault zone disturbance, unit 314 is broken into pieces, vertical offset across the fault zone, and wedge shaped thickness of unit 313, thickened near the fault zone (**M**).
	T07E	13–15	fz and cw	316	311	Units 318–316 are heavily disturbed and broken in pieces. Wedge-shaped unit 312 is 3 times thicker near the main fault zone than outside (**W**).
	T09W	5–6	cw, au, and tb	313	311	Blocks containing unit 313 are tilted to vertical and doubled between fault branches. The wedge-shaped unit 312 is thicker in the fault zone than outside. The flat-lying unit 311 covers the fault zone (**S**).
H	T09E	~3	vo and fz	400	313	The top of unit 400 is clearly offset, but fault termination level is not clear (**M**).
	T07E	12–14	fz, ut, and tc	319	317	Fault zone with multiple shearing surfaces. Base of unit 318 is offset. The combined thickness of units 317–313 is 20 cm thicker on the footwall (**F**).
	T09W	4–5	vo	319	314–316	Sharp offset of unit 319, fault trace terminating within unit 317 (**S**).
		6–7	ut	400	316	Shearing surface in unit 400, whose upper boundary is being offset (**W**).

[a]Abbreviations for types of event indicators used in this table (following those in *Scharer et al.* [2007]) include au, angular unconformity; cw, colluvial wedge; fc, facies change; fd, folding of units; fis, fissures; fz, fault zone; mt, mole track; sf, shearing fabric; tb, tilted or overturned blocks; tc, thickness change; ut, upward termination; vo, and vertical offset. Rating of event evidence includes **W**, weak; **M**, moderate, alternative interpretation is possible; **F**, fair; and **S**, strong.

Table 3. Radiocarbon Ages From the Salt Lake Site, Haiyuan Fault

Sample Name	Laboratory Number[a]	Unit	^{14}C Age[b]	±	Trench Wall[c]	Material	Calibrated Age (2σ)[d]	Modeled Age (Posterior)[d]
SL07-33	AA80268	106	162	35	07W	Charcoal	1663–1953 A.D.	1858–1955 A.D.
SL07-34	AA80269	107	145	35	07W	Charcoal	1667–1950 A.D.	1830–1947 A.D.
SL07-47	AA80270	112–114	6929	47	07W	Charcoal	5722–5970 B.C.	/
SL07-35	GU-18151	110–112	115	30	07W	Charcoal	1680–1939 A.D.	1802–1928 A.D.
SL07-84	AA80271	121	159	39	07EE	Charcoal	1663–1953 A.D.	1749–1886 A.D.
SL07-54	AA80272	122	57	64	07W	Charcoal	1677–1941 A.D.	1722–1851 A.D.
SL07-45	GU-18142	123	215	30	07W	Charcoal	1644–1955 A.D.	1754–1877 A.D.
SL07-21	GU-18150	123	42045	6300	07E	Charcoal	/	/
SL07-05	GU-18146	125–126	49640	1575	07E	Charcoal	/	/
SL07-13	AA80273	126	40600	1300	07W	Charcoal	/	/
SL07-44	GU-18149	200	150	30	07W	Charcoal	1667–1951 A.D.	1685–1820 A.D.
SL07-68	GU-18148	202a	155	45	07E	Charcoal	1664–1952 A.D.	1672–1795 A.D.
SL07-64	AA80274	202a	203	34	07E	Charcoal	1643–1955 A.D.	1679–1775 A.D.
SL07-71	GU-18152	203	100	30	07E	Charcoal	1682–1935 A.D.	1671–1732 A.D.
SL07-55	AA80277	212	288	43	07W	Charcoal	1477–1797 A.D.	1534–1665 A.D.
SL07-69	GU-18145	212 base	475	45	07E	Charcoal	1321–1615 A.D.	1559–1632 A.D.
SL09-23	UCI-119446	215	3925	50	09E	Charcoal	2234–2570 B.C.	/
SL09-25	UCI-119447	216a (upper)	300	15	09E	Charcoal	1521–1648 A.D.	1517–1589 A.D.
SL09-24	UCI-119448	216b (lower)	390	15	09E	Charcoal	1446–1615 A.D.	1446–1510 A.D.
SL09-13	UCI-119449	301–302	1060	15	09E	Charcoal	902–1020 A.D.	976–1021 A.D.
SL07-02	GU-	303	1040	30	07E	Charcoal	898–1033 A.D.	897–1015 A.D.
SL09-18	UCI-119450	307	2190	30	09E	Charcoal	176–365 B.C.	/
SL07-78	AA80279	308	1692	43	07E	Charcoal	240–430 A.D.	240–431 A.D.
SL09-20	UCI-119451	310	2225	20	09E	Charcoal	206–381 B.C.	205–381 B.C.
SL07-74	AA80280	311–312	3086	38	07E	Charcoal	1265–1432 B.C.	1264–1433 B.C.
SL07-72	AA80281	317	3654	39	07E	Charcoal	1918–2141 B.C.	1919–2141 B.C.
SL09-29	UCI-119452	318	3865	15	09W	Charcoal	2287–2460 B.C.	2234–2431 B.C.
SL09-04	UCI-119453	319	3865	15	09W	Charcoal	2287–2460 B.C.	2306–2461 B.C.
SL09-30	UCI-119454	320	4075	20	09W	Charcoal	2497–2839 B.C.	2494–2530 B.C.
SL09-31	UCI-119455	400	3875	20	09W	Charcoal	2922–2461 B.C.	2536–2559 B.C.
SL09-34	UCI-119456	below 400	2805	20	09W	Charred root	907–1008 B.C.	/

[a]Samples processed at the Arizona AMS Laboratory (AA); University of Glasgow, UK (GU); and Keck Carbon Cycle AMS Facility, UC Irvine (UCI).
[b]The quoted age is in radiocarbon years using the Libby half-life of 5568 years and following the conventions of Stuiver and Polach [1977].
[c]Trench exposure: 07E or 07W: east or west wall opened in 2007 field season; 07EE: exposure ~1 m east of east wall of 2007 field season; 09E or 09W: east or west wall in 2009 field season.
[d]Outlier samples, either too old due to apparently reworked or in two cases too young, are not used in age modeling and denoted with "/."
[e]All of the samples have been pretreated with an acid-base acid-wash to remove contamination and secondary carbonates. Sample preparation backgrounds have been subtracted, based on measurements of ^{14}C-free wood.

be stratigraphically lower than the actual event horizon [e.g., *Bonilla and Lienkaemper*, 1990; *Rockwell et al.*, 1986] or that water laden sediments of the top layers fold rather than fault during earthquake rupture.

5.4. Less Likely Events

If the upward termination of fault branches can stop below the event horizon, then such criteria should probably not be used alone to define an event [e.g., *Weldon et al.*, 2002; *Scharer et al.*, 2007]. To illustrate the consequence of this uncertainty, we denote event B for some weak evidence of cracks stopping at unit 110. For instance, in exposure T09E (Figures 8a and 8c], it corresponds to a short-fault segment that offsets sharply units 129–110 with 10 cm in vertical separation but with a reduction in the offset upsection to zero. Warping of units between this short fault and the one in the main fault zone suggests that it could be soft-linked with, and jump to, a strand ~50 cm to the south that reaches the surface, resembling en echelon arrangement of fault segments seen in map view. In exposure T07EE, the evidence for event B is also in the form of upward termination of fault branch with nominal offset (Figure 7e). We interpret this rootless fault to be formed by the 1920 earthquake rupture, rather than a distinct, older event.

There is a remote possibility of a separate event D at a stratigraphic level slightly lower than event C, in unit 127. Unlike evidence for event C, which includes brittle faults, folding, and unconformity, event D would be associated with only upward termination of faults with diminishing offset. As shown in exposure T07W, a forked

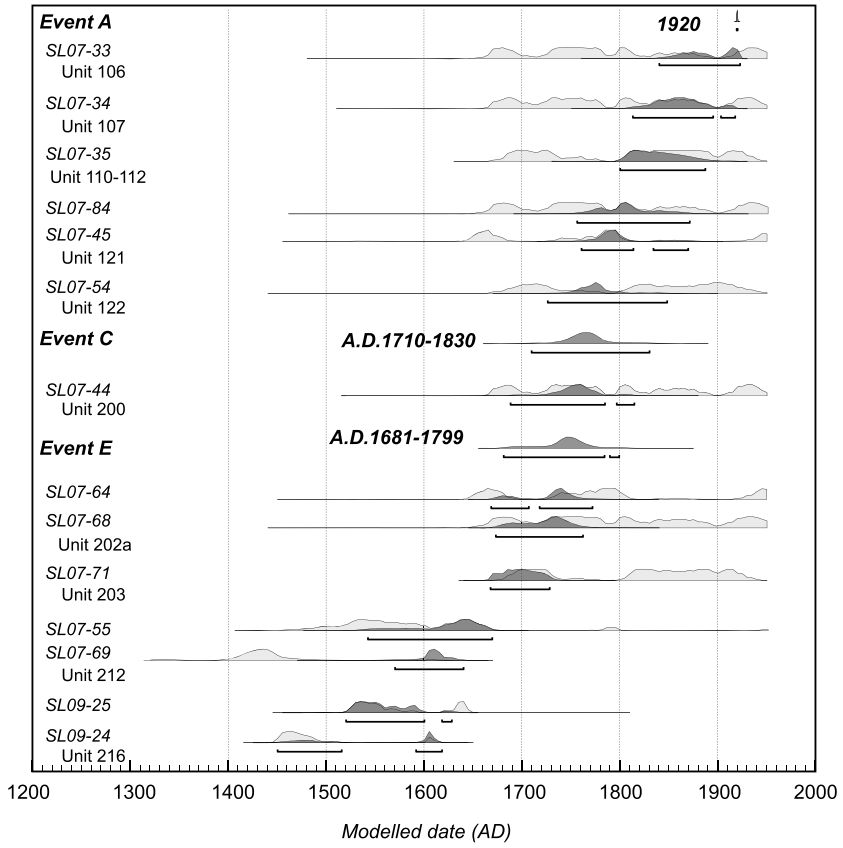

Figure 9. OxCal modeling of charcoal ^{14}C ages in stratigraphy and constraints on timings for (a) surface-rupturing events A (1920), C, and F and (b) older events F, G, and H. Prior probability distribution functions (PDFs) for radiocarbon samples are shown in light gray and posterior PDFs shown in dark gray. Corresponding unit numbers containing charcoal samples are shown on the shaded bars. Modeled earthquake ages shown by PDFs and labeled by event name. OxCal modeling v4.2.1 with atmospheric data from *Reimer et al.* [2009].

secondary fault branches off in two strands, with one being traced to unit 123 (event C) and the other disappearing at a lower level, within unit 127 (Figure 6b). Similarly, in the main fault zone, a strand branches off toward the hanging wall and stops shortly above unit 129 but does not disrupt overlying unit 122 (Figure 6c). Nevertheless, given the small stratigraphic separation between these upward terminations, a conservative interpretation would be that D is not an independent event. Instead, the expressions of event D are upward terminations of faulting formed during event C.

In summary, event A is the strongest in evidence with various patterns of deformation and vertical separation up to 20–50 cm across faults in the trench. In contrast, events C and E are associated with only a few to ten

Table 4. Summary of Modeled Event Dates at the Salt Lake Site, the Haiyuan Fault

Events	A	C	E	F	G	H
95% age range[a] Model 1[b]	/	1710–1830	1681–1799	/	/	/
95% age range Model 2[b]	/	1685-1778	1663–1748	350–986	B.C. 1325–2031	B.C. 1985–2351
Candidate historical earthquakes	1920	1760 or 1709	1638	/	/	/

[a]All ages are in A.D. unless labeled otherwise.
[b]In model 1, only samples within the upper stratigraphic section (above unit 300, which contains a depositional hiatus and a shift to lower sedimentation rate) were used to constrain event dates. In model 2, samples from the entire trench-exposed stratigraphy were used (unit 102 through unit 400; shown in Figure 4).

centimeters of vertical offset, yet are observable, as distinct due to coupled fault terminations and folded layers underlying growth strata. Events B and D are both unlikely to be separate earthquakes, because these consist only of upward fault terminations that may be associated with events A and C, respectively. Of these two, event D is more likely to be a distinct event than B. Thus, there is strong evidence for three events within the upper section, with low potential for a fourth event.

For older events F, G, and H, we list the evidence for individual events in Table 2 and show the interpretations in the corresponding trench logs in Figures 5–8, without elaborating on the details.

6. Event Age Determination

Ages of the paleoseismic events at the Salt Lake site are constrained both by radiocarbon dates of charcoal retrieved from the trenches and historical accounts of earthquake shaking in the region.

6.1. Radiocarbon Dating of Earthquakes

Charcoal is abundant in the trenches. Seventeen radiocarbon samples collected within the upper section, all detrital charcoal, were sent for accelerator mass spectrometer (AMS) dating to three different laboratories. The results are consistent among laboratories and summarized together here in Table 3. The stratigraphic positions of the samples are shown in the composite stratigraphic column (Figure 4). The majority of samples are in correct stratigraphic order, with increasing ages with depth, suggesting high reliability. Some samples yield dates much older (up to 40,000 years B.P.) and out of stratigraphic order, suggesting some reworking, which is common for detrital charcoal (marked as italic in Table 3). Consequently, we do not use these samples to develop chronologic models for event ages. Overall, the dates suggest that the upper section was deposited during the last 500 years, with a rapid average sedimentation rate of ~5 mm/yr.

OxCal modeling of 14 radiocarbon ages [*Bronk Ramsey*, 2013] provides age control of event occurrence, suggesting that events A, C, and E all occurred sometime after A.D. 1600 (Figure 9). Among the total of 19 dated charcoal samples within the upper section layers, five samples are much older and out of stratigraphic order, thus not used in constraining event ages. As previously discussed, we interpret most recent event A being the historical 1920 earthquake. Events C and E occurred most likely sometime in the time window A.D. 1710–1830 and A.D. 1681–1799 (2σ), respectively (Figure 9 and Table 4). OxCal modeling of event date ranges could possibly vary depending on the choice of stratigraphic sequence for age constraints. Table 4 lists the results of using the upper stratigraphic section, in comparison with those constrained by the entire exposed stratigraphy. The difference is small.

Three older events F, G, and H, exposed in the lower section of our trenches, are constrained to occur during A.D. 350–986 (2σ), B.C. 1325–2031 (2σ), and B.C. 1985–2351 (2σ), respectively (Table 4). These three events, plus event A (1920), are broadly consistent with the most recent four events at the Gaowanzi site, ~15 km west of our site [*Ran et al*., 1997] (GWZ; Figure 1b). Thus, the time intervals between these events are 1252 ± 318, 2346 ± 475, and 490 ± 397 years, respectively, which show considerable variation. Comparing with previous results at the Gaowanzi site, the centimeter-resolution stratigraphy of the upper section at the Salt Lake site reveals more and probably smaller events during the last 500 years.

6.2. Historical Accounts of Earthquake Damage

Historical documents provide independent information to constrain the timing and magnitude of events recognized in trenches [*Marco et al*., 1997; *Wen et al*., 2008; *Ambraseys*, 2009; *Sapkota et al*., 2012; *Klinger et al*., 2015]. The long written history of China has produced one of the longest and most complete records of historical seismicity in the world, with the very first account of earthquake damage dated back to 23rd century before the Common Era [*Xie and Cai*, 1983]. Since the Yuan dynasty (A.D. 1271–1368), local annals and records at provincial, prefectural, and county levels became common, resulting in an increase in both the number and content of documented seismic events.

A comparison of our paleoseismic record with historical earthquake accounts is possible for the Haiyuan Fault, as written documents of earthquake effects in the region date back to 190 B.C. [*Xie and Cai*, 1987a, 1987b]. Searching through various Chinese historical documents for local accounts of earthquake damages, we established a comprehensive list of all accounts of earthquakes that affected towns closest to our trench site (Table 5). From these historical records, we could further narrow down the dates of paleoearthquakes

Table 5. List of All Entries of Earthquakes in Official Documents of Jingyuan and/or Haiyuan Between A.D. 1352–1919

Date of EQ[a]	Written Account of Earthquake Damage Type of Damage or Felt	Original Source of Historical Documentations (Local, Provincial, and Central Annals)	Comments[e]	Epicenter Location Inferred	Catalogs That List the Earthquake[b]
2 April 1760[c]	**On the day of 27 February (in the lunar calendar) of the 25th year of Qing Emperor Qian Long, ground shaking in *Haiyuan*.**	**Annals of Zhenyuan county, volume 7, page 5. and Gansu Tong Zhi, Book Anomalies, Section earthquakes, page 37 l.**	**This earthquake was not included in most catalogues due to brevity of damage report OR paucity of reports for this event. Magnitude difficult to evaluate.**	**Near Haiyuan**	**5 and 6**
3 January 1739	24 November (in the lunar calendar) of the 3rd year of Qing Emperor Qian Long, ground shaking severely with sounds, more shocks sporadically, and last more than a month.	Annals of ***Jingyuan*** County, Section Auspiciousness and Anomalies, page 7 (or page 94[d])	This earthquake was named the great 1739 Pingluo M 8 earthquake[catalog 3], whose epicenter is 400 km southeast of the Salt Lake.	Pingluo, Ningxia	1–8
30 January 1710	On the day 1 January (lunar calendar) of the 49th year of Qing Emperor Kang Xi, earthquake Ground shaking again (possibly referring to the 1709 earthquake previous year) on the on 1 January in ***Jingyuan*** and ***Yongdeng***	Annals of ***Jingyuan*** prefecture, Volume 1, Page 4 (or page 92[d])	Not sure whether it was one earthquake felt and recorded in both towns, and two separate ones. Could be an aftershock of the 1709 Zhongwei earthquake.	Unclear	5 and 6
14 October 1709	On the day of 12 September (lunar calendar) of the 48th year of Qing Emperor Kang Xi, severe ground shaking, with sounds. >2000 civilian houses collapsed, >20 piers, city wall collapsed for more than 166 Zhang and 7 Chi long, 32 people died. More shaking occurred months afterward.	Annals of ***Jingyuan*** County, Section Auspiciousness and Anomalies, volume 1, Page 4 (or page 92[d])	14 October 1709 Zhongwei M $7_{1/2}$ earthquake occurred on the Zhongwei Fault, which is subparallel to the Haiyuan Fault to the north [e.g., *W. Zhang et al.*, 1988]. See Figure 1 for location.	Zhongwei	1–8
	Guyuan prefecture: in the 49th year of Qing Emperor Kang Xi, the Zhengshui general (stationing at ***Guyuan***) Pan Yulong rebuilt 24 towers of various heights, and outer city walls for 13.7 Li long, and 3.6 Zhang high.	and Gansu Tong Zhi, Volume 7, Page 10u	One Zhang is about 3.33 m, and one Chi is about 0.33 m, one Li is about 0.5 km.		
14 October to 1 November 1708 (1709)[c]	**On the day of autumn September (lunar calendar) of the 47th year of Qing Emperor Kang Xi, ground shaking in *Xi'an Zou*, water springs dried up.**	**Annals of Haicheng County annals, Volume 7, Page 2**	**In most catalogs, this item was considered a transcript error, mistaken of 14 October 1709 Zhongwei M $7_{1/2}$ earthquake[catalog 3].**	**None**	**1 and 6**
January 1638[c]	**On the day of December (lunar calendar) of the 10th year of Ming Emperor Chong Zheng, *Haichi* (now *Haiyuan*) and *Xi'an Zou* (a village 20 km east of Salt lake, and similar distance to Haiyuan, now village, old city walls still preserved), ground shaking in both towns, on the same day. More shaking occurred afterward and lasted a few months.** **City walls, piers, and civilian houses all collapsed[catalog 4].**	**Ming Dynasty Annals–Books Wu Xing, Volume 3 and Described in Gu (ed.) catalog[catalog 4], but original**	**Estimated intensity VI in the "epicenter region." Estimated magnitude $5_{1/2}$[catalog 3]**	**Between Salt Lake and Haiyuan**	**1–8**

Journal of Geophysical Research: Solid Earth

10.1002/2015JB012163

Journal of Geophysical Research: Solid Earth

10.1002/2015JB012163

Table 5. (continued)

Date of EQ[a]	Written Account of Earthquake Damage Type of Damage or Felt	Original Source of Historical Documentations (Local, Provincial, and Central Annals)	Comments[e]	Epicenter Location Inferred	Catalogs That List the Earthquake[b]
		historical document source was not specified.			
16 May 1597	On the day of 1 April (also Xinjiu Suo in the lunar calendar) of the 25th year of Ming Emperor Shen Zong (Wan Li), Earth shaking in ***Gansu*** and ***Xi'an Suo*** (***Zou***).	Ming Dynasty Annals–Books Wan Li, Volume 309, Page 1.	Two interpretations: one considered that Xi'an Suo should be Xi'an Zhou. The other considered that Xi'an Zhou should be Xining Zhou, due to a transcription error. Because of the ambiguity, this event was not considered a reliable earthquake record and not included in most catalogs.	Unclear, could be somewhere in the Qilian Shan.	1 and 6
7 July 1590	On the day of 6 June (lunar calendar) of the 18th year of Ming Emperor Shen Zong (Wan Li), ground shaking, with rain and snow in ***Jinglu Wei*** (now ***Jingyuan***).	Lanzhou Provincial Annals (Qing Emperor Dao Guang), Volume 12, Page 6.	This earthquake likely occurred more to be near Lintao than Jingyuan. The description of ground shaking in Jingyuan is more likely describing the thunders accompanying the unusual storm, despite temporal coincidence with those in Lintao.	Near Lintao	1, 5, 6, and 8
	(The same day), Didao (now ***Lintao***, a town 250 km southwest of the Salt Lake site) also ground shaking, city wall collapse, civilian and animal casualties.	and			
	On the day of 6 June (lunar calendar) of the 18th year of Ming Emperor Shen Zong (Wan Li), ground shaking with snow in the height of summer time.	Annals of ***Jingyuan*** County, Section Auspiciousness and Anomalies, page 88[d]; (Kang Xi version) volume 1, page 3.			
9 October 1588[c]	On the day of 19 August (lunar calendar) of the 16th year of Ming Emperor Shen Zong (Wan Li), thundering and ground shaking, more than Chi-deep snow cover in ***Jinglu Wei*** (now ***Jingyuan***).	Annals of ***Jingyuan*** County, Section Auspiciousness and Anomalies, page 88[d]; (Kang Xi version) volume 1, page 3.	It is possible that the ground shaking described was not earthquake-induced shaking, rather the thunders accompanying an unusually intense snow storm.	none	1, 5, and 6
25 July 1561	14 June (in the lunar calendar) of the 46th year of Qing Emperor Jia Jing, at the hour of Wu Shi (roughly 11:00 AM–1:00 PM), ground shaking. More quakes lasted more than 20 days, upsetting local inhabitants.	Annals of ***Jingyuan*** County, Section Auspiciousness and Anomalies, page 86[d]. (Kang Xi version) Annals of Jingyuan county, volume 1, page 2.	This earthquake was named the great 1561 Zhongwei M $7_{1/4}$ earthquake[catalog 3], whose epicenter is 100 km north of the Salt Lake.	Zhongwei	1–8
	In ***Guyuan***, ground shaking in mid-June, over 1000 ranching families death from building collapse, in addition to more than 500 horses.	and Jia Jing Factual Records, volume 503, page 3.			
	In ***Guyuan***, ground shaking and fissures	and Gansu Tong Zhi (by Xu Rong, of the Qing dynasty), volume 24.			
23 January 1556	In the 34th year of Ming Emperor Jia Jing, ground shaking severely, with sounding.	Annals of ***Jingyuan*** County, Section Auspiciousness and Anomalies, page 85[d]	This earthquake was named the great 1556 Huaxian M $8_{1/4}$ earthquake[catalog 3], whose epicenter is 400 km southeast of the Salt Lake.	Huaxian	1–8
4 November 1542	On September Jiawu (in the lunar calendar) of the 21th year of Ming	Jia Jing (Ming Emperor) Factual Records, volume 226, page 5.	The felt region for this earthquake is large. If one draws a circle to include	Near Haiyuan?	6

Table 5. (continued)

Date of EQ[a]	Written Account of Earthquake Damage Type of Damage or Felt	Original Source of Historical Documentations (Local, Provincial, and Central Annals)	Comments[e]	Epicenter Location Inferred	Catalogs That List the Earthquake[b]
	Emperor Jia Jing, Earth shaking with thunders in ***Pingyang*** county of Shannxi, ***Guyuan*** Counties, and Ningxia, Taozhou of Shanxi		all reported towns, Haiyuan would be near the center.		
30 August 1542	In July Wucheng of the 21th year of Ming Emperor Jia Jing, in ***Jinglu Wei*** (now ***Jingyuan***), Shanxi, ground shaking with thundering sounds.	Shi Zong (Ming Emperor) Factual Records, volume 264, page 8. and Guoque (by the great historian Shima Qian), Volume 57, Page 3630.	Most earthquake catalogues do not include this earthquake entry.	Unclear	1 and 6
23 June 1540	*On May Gengzhi of the 19th year of Ming Emperor Jiajing, earthquake shaking in* ***Guyuan*** *and other counties.*	*Jia Jing (Ming Emperor) Factual Records, volume 237, page 2.*	Most earthquake catalogues do not include this earthquake entry.	*Near Guyuan*	*5 and 6*
10 April 1495	On March Xinchou of the 8th year of Ming Emperor Hong Zhi, ***Jinglu Wei*** ground shaking, accompanying sound of thunders. In March Xinchou of the 8th year of Ming Emperor Hong Zhi, in ***Jinglu Wei***, Shanxi, ground shaking with thundering sounds. Repeated ground shaking in Ningxia until Ren Yin Liu Xian.	Xiao Zong (Ming Emperor) Factual Records, Volume 98, Page 5. and Guoque (by the great historian Shima Qian), Volume 43, Page 2672.	This earthquake was considered to be located to be east of Zhongwei, Ningxia (100 km north of the Salt Lake), with main shock magnitude estimated $6_{1/4}^{\text{catalog 3}}$ (earthquake sequence, with clear record of foreshock and aftershock sequences). Estimated magnitude $6_{1/4}$ (with intensity of VIII)$^{\text{catalog 3}}$	East of Zhongwei	1–8
21 April 1491	*On the day of Yichou March (i.e., 13 March) of the 4th year of Ming Emperor Hong Zhi,* ***Jinglu Wei*** *(now* ***Jingyuan****), and* ***Gan Yanci*** *(i.e.,* ***Salt Lake****) Earth-shaking with roaring sound from the underground.*	*Xiao Zong (Ming Emperor) Factual Records, Volume 49, Page 6.* *and* *Guoque (by the great historian Shima Qian), Volume 42, Page 2626.*	*Both Jingyuan and Salt Lake felt the shaking, suggesting that the earthquake may occur somewhere in between, if on the Haiyuan fault.*	*Between Jingyuan and Salt Lake*	*1,5, and 6*
18 April 1352	March of the spring in the 13th year of Ming Emperor Zhi Zheng, earthquake in ***Longxi***, government building collapsed, aftershocks lasted more than 100 days.	Annals of ***Jingyuan*** County, Section Auspiciousness and Anomalies, Page 83[d]	Longxi is ~160 km south of Jingyuan. This earthquake was named as Longxi earthquake, with magnitude estimated to be $M\ 7^{\text{catalog 3}}$	Longxi	1–8

[a]Dates are converted to western calendar from Chinese traditional dynastical date and lunar calendar.
[b]Catalogs referred to (1) *Committee of Earthquake Research, Academia Sinica* [1956], (2) *Li* [1960], (3) *Central office of Earthquake Working Group* [1971], (4) *Gu* [1983], (5) *Xie and Cai* [1983, 1985, 1987a, 1987b], (6) *LIER* [1989], *NBCEA* [1988], (7) *IGCEA and HGFU* [1986, 1990], and (8) *DEMPSSB* [1995].
[c]Most likely candidate earthquakes for paleoseismic events in trenches exposed at the Salt Lake are highlighted in bold. Less likely candidates, which cannot be ruled out, are shown in italic and bold.
[d]Page number in the 1925 print version of the Annals of Jingyuan County.
[e]For historical earthquakes, magnitude cannot be accurately estimated down to the decimal level. Chinese catalogs use subdivides of 1/4, 1/2, and 3/4 to differentiate the sizes between whole numbers.

AGU Journal of Geophysical Research: Solid Earth

10.1002/2015JB012163

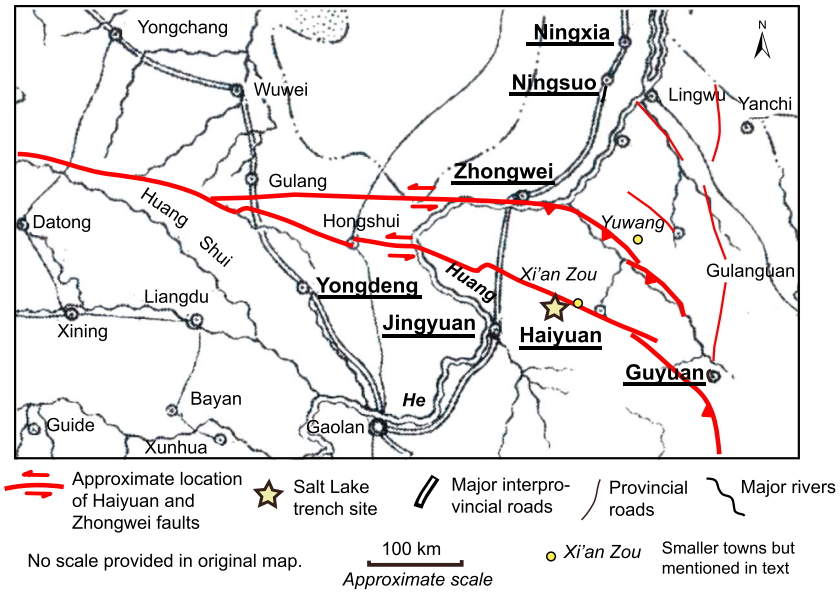

Figure 10. Major villages and towns near the Salt Lake trench site during the Ming and Qing dynasties (modified from *Zhang* [1934]).

exposed in our trenches. Within the time window for event occurrence permissible from OxCal modeling, the most probable dates for the three earthquakes exposed are A.D. 1920, 1760, (or 1709) and 1638, from the youngest to oldest. There is little doubt that the most recent event A is the stratigraphic evidence of the 1920 Haiyuan earthquake.

It is possible that the locally recorded A.D. 1760 earthquake is the penultimate event (event C) exposed at the Salt Lake site. The A.D. 1760 earthquake was recorded only locally in the town of Haiyuan (population of ~180,000 in mid-1700) (Table 5) [*Committee of Earthquake Research, Academia Sinica*, 1956] and not recorded in other towns in the region. It was written as "ground shaking in Haiyuan"; however, this brief description should not be considered as a merely shaking in the modern sense. First, in ancient China, earthquakes were considered bad omens to some extent, such that official documents tended not to record earthquake unless the damage was severe enough to be inescapable. Second, material for written documentation was an expensive commodity centuries ago. There is a tendency for documents being written in concise language, in contrast with modern voluminous detailed documentation, so that details were lost or minimized.

A less likely scenario, which is permissible with OxCal modeling of event occurrence, is that event C might represent the remote effect of the A.D. 1709 earthquake. The seismogenic fault for the A.D. 1709 earthquake was considered to be the Zhongwei Fault, subparallel to the Haiyuan Fault in the north, and ~100 km north of the Salt Lake site [*Zhou and Liu*, 1987; *W. Zhang et al.*, 1988; *Nie and Lin*, 1993]. It was assigned magnitude $7_{1/2}$ and was widely recorded in towns within a 500 km radius region of intensity VI [*Gu*, 1983; *IGCEA and HGFU*, 1990]. Our trench site is within the region of assigned intensity of VIII. At Xian Zhou, ~20 km east of the Salt Lake site, the 1709 earthquake was recorded, as "ground shaking, with water springs dried up." If the penultimate event exposed at the Salt Lake site was the consequence of the 1709 Zhongwei M $7_{1/2}$ earthquake, it could be triggered cracking on the Haiyuan fault, similar to the response of the faults in the Salton Sea region, Southern California, to earthquakes on nearby faults [*Hudnut et al.*, 1989; *Rymer et al.*, 2002, 2010; *Wei et al.*, 2011].

The A.D. 1638 earthquake appears to be the best candidate earthquake falling within the OxCal modeling date range for event E. The 1638 earthquake was described as "city walls and civilian houses all collapsed, in both Haiyuan and Xian Suo (Zou). Aftershocks lasted a few months" (Table 5). Thus, this earthquake was recorded in two known towns ~20 km apart along the western section of the Haiyuan Fault but was not recorded in other bigger and more populated towns in the region, such as Guyuan, Zhongwei, or Jingyuan (Figure 10).

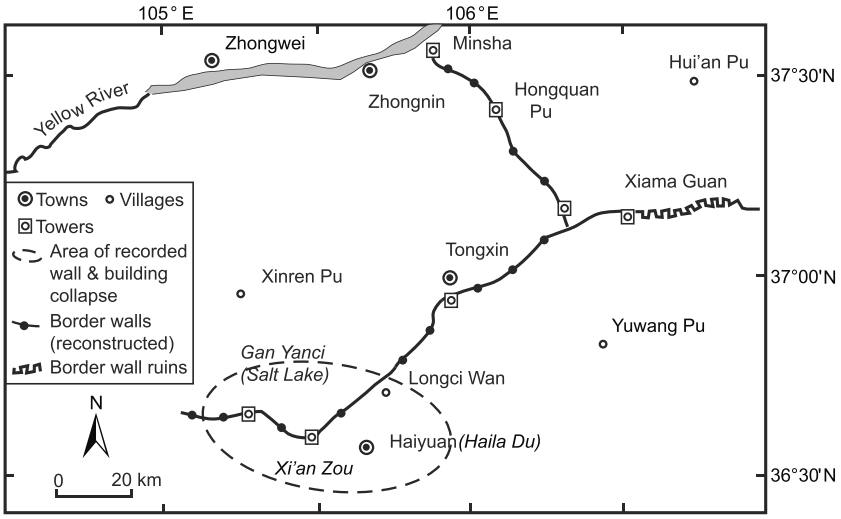

Figure 11. Map showing locations of border walls near Haiyuan, which was one of the border outposts in the Ming and Qing dynasties. Dash-outlined ellipse denotes area of reported complete collapse of border walls, which except fortress ruins in Gan Yanci and Xi'an Zou, due to shaking of A.D. 1638 earthquake.

7. Event Size Estimation

Despite the fact that the most recent event A, the 1920 Haiyuan earthquake, was approximately *M* 8, written historical records suggest that it is unlikely that a similar 1920-type magnitude 8, or even magnitude 7, has occurred on the same section of the Haiyuan Fault during the past 500 years [*Gu*, 1983; *Xie and Cai*, 1987a, 1987b]. This inference is based on comparing the severity of damage and the size of the area where the earthquake was felt in the same region and during the same era.

Conversion of felt effect to intensity and then to magnitude adds additional uncertainty [*Gu*, 1983]. The level of documentation depends on the population: less in remote areas than in or close to bigger villages/towns. All these factors tend to result in incompleteness of earthquake recording, particularly of those small in magnitude and without severe damage. In general, the smaller in size and earlier in time an earthquake occurred, the less likely the earthquake magnitude can be quantified. Even for those recorded, damage effects may be either simplified or details minimized or completely omitted from official documents. Information is often too scarce to adequately quantify isoseismals and/or seismic intensity for earthquakes smaller than 7 or for those that occurred prior to the Qing dynasty (A.D. 1636–1912) to attempt sophisticated analysis of *Bakun and Wentworth* [1997].

Nonetheless, large to strong earthquakes of known (agreed upon) magnitude in the area during the same period of time can be used as references to estimate those of unknown magnitude. For instance, the 10 April 1495 *M* $6_{1/4}$ Zhongwei earthquake was felt and recorded in Jingyuan [*Gu*, 1983] (Table 5). Conversely, if an earthquake of similar magnitude occurred near the Salt Lake basin, it would cause damage severe enough to warrant a recording at Zhongwei, which was a larger town than Jingyuan (Figure 10), baring the difference in rupture directivity and site effects. Since none of the three Salt Lake historical earthquakes were recorded at Zhongwei, they were probably smaller than *M* $6_{1/4}$. Of the two candidate earthquakes in A.D. 1760 and 1638, shaking effects were recorded only in a few towns within 50 km from the trench site (Figures 10 and 11). Compared to the large felt region of 500 km from Haiyuan associated with the 1920 *M* 8 event [*LIS and NBCEA*, 1980], this indicates that the magnitude of these events had to be significantly smaller than 8. The felt-recorded region of the 1638 earthquake is also smaller than that of A.D. 1622 *M* 7 Guyuan earthquake (Figure 12), whose shaking was recorded in more populated towns ~230 km to the southeast. Reconstructed isoseismals of the 1622 earthquake suggest a large felt region, with maximal intensities IX–X in a region of ~75 km in long axis [*IGCEA and HGFU*, 1986].

In some versions of Chinese catalogs of historical earthquakes, the 1638 earthquake was listed with a magnitude of $5_{1/2}$ [*Gu*, 1983; *IGCEA and HGFU*, 1986], which is likely to be an underestimate. Recent studies of some moderate to strong earthquakes suggest that the magnitudes of historical earthquakes in Chinese catalogs

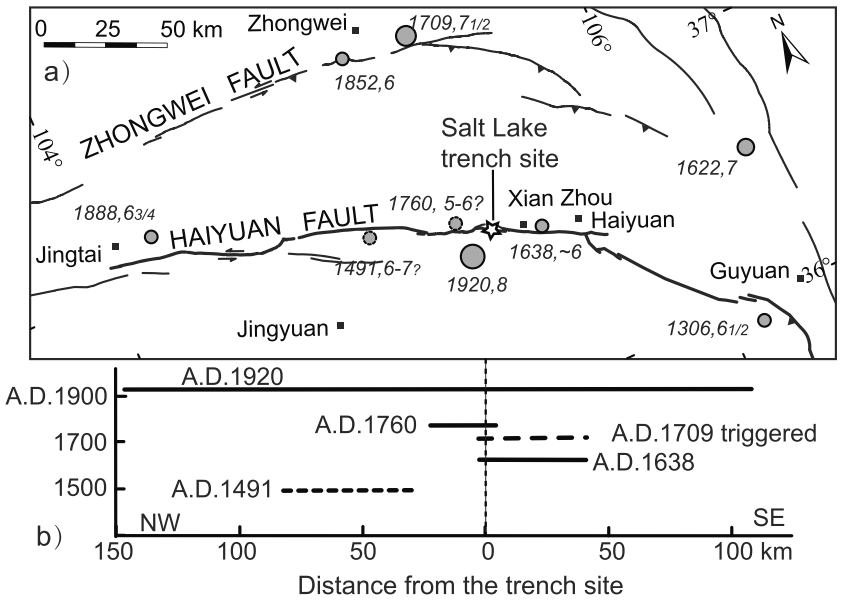

Figure 12. Scenarios of rupture extents for paleoearthquakes identified in the Salt Lake trenches. (a) Map view of Haiyuan and Zhongwei Faults, catalogued historical earthquakes of magnitude 6 and above. Surface ruptures of the 1920 earthquake are highlighted in bold. (b) Possible rupture scenarios for earlier paleoseismic events. Considerably shorter ruptures, on the order of 10–30 km and 40–60 km for A.D. 1760 and 1638 earthquake, respectively. Dashed line denotes an alternative of the 1760 earthquake, possibly triggered slip on the Haiyuan Fault, induced by A.D. 1709 earthquake, which occurred on the south dipping Zhongwei Fault, 70 km to the north. A.D. 1491 earthquake, which was felt in both Jingyuan and Salt Lake, was not recorded in our trenches. Rupture scenarios shown are highly speculative, due to a paucity of data.

can be underestimated by 0.5–1 unit [*Yuan et al*., 2007]. Furthermore, A.D. 1634 is 10 years before the demise of the Ming dynasty; textual recording of earthquake could be overlooked in towns where shaking was not severe enough. Nonetheless, our new investigation of informal writings and tomb scripts suggests that in addition to collapse of city walls and civilian houses, a long stretch of border fortress from Tongxin to Xian Suo (Zou) was destroyed during this earthquake; thus, considerable damage occurred in a region about ~65 km in long axis along the Haiyuan Fault (Figure 11). In *Gu* [1983] and Chinese seismic intensity scale [*NQTSA*, 1999], the description "all city walls and civilian houses collapsed" indicates a seismic intensity of VIII in Haiyuan City. The assignment of intensity was highly empirical, and based on macroscale damage pertain to Chinese-style construction and buildings. Similar to the modified Mercalli intensity scale, a scale of 12 levels of seismic intensities was used, as summarized in Chinese seismic intensity scale [*NQTSA*, 1999], which was developed upon earlier versions. The best estimates of equivalent peak ground acceleration and peak ground velocity for each level of intensity are also given in *NQTSA* [1999]. Considering that the Haiyuan town was likely a few tens of kilometers from the epicenter, the epicentral intensity (I_o) could be higher, VIII to IX. Using the empirical relationship of $M_s = 0.605\ I_o + 1.376$ for western China [*DEMPSSB*, 1995] or earlier version $M_s = 0.58\ I_o + 1.5$ [*Gu*, 1983] suggests an estimation of $M_s = 6.2$–6.8. That "aftershocks lasted a few months" suggests that the magnitude of 1638 earthquake was probably above 6.

No magnitude was previously assigned to the 1760 earthquake because of the scarcity of descriptions, but it is very likely to have been smaller than the 1638 event, if the felt region was smaller. Given that the earthquake was not recorded in larger towns 100 km away, it was probably smaller than $M\ 6_{1/4}$. Nonetheless, it is very speculative to assign a magnitude to the A.D. 1760 earthquake, given the scarcity of information.

Given possible systematic underestimation in magnitude and our own investigation of historical documents, we estimate the magnitude of the 1638 earthquake to be M_s 6.2–6.8, possibly approaching M 7, and the 1760 earthquake to be even smaller. Hence, the multievent sequence at the Salt Lake paleoseismic site consists of earthquakes rather heterogeneous in magnitude, from low to mid-6 to near 8.

Based on estimates of earthquake magnitude and fault segments defined by geometric complexities [*Wesnousky*, 2006; *Klinger*, 2010], we construct a speculative rupture scenario for earthquakes identified in the

Salt Lake trenches (Figure 12). It is well constrained that surface rupture of the 1920 earthquake is a multisegment long rupture [e.g., *Deng et al*., 1986]. In contrast, based on the empirical relationship [*Wells and Coppersmith*, 1994; *Wesnousky*, 2008], the earlier events were considerably shorter ruptures, on the order of 40–60 km and 10–30 km, for the 1638 and 1760 earthquakes.

8. Discussion

The Salt Lake record demonstrates that local moderate-magnitude earthquakes, when breaking to the surface, can be preserved if the stratigraphy is suitable. These ruptures are associated with submeter to a few centimeter ground deformation [e.g., *Wells and Coppersmith*, 1994; *Wesnousky*, 2008], which are difficult to observe without centimeter-scale resolution stratigraphic control. The upper ~2.7 m thick section at the Salt Lake site consists of 60–70 layers with centimeter to millimeter in thickness, deposited during the last 400–500 years. Hence, this site provides optimal conditions to record centimeter-scale offsets, similar magnitude warping and subsequent growth strata, and separation of different event horizons. Although of lower probability, we should not exclude the possibility of finding evidence of local moderate-magnitude earthquakes in trenches. Data are cumulating. For instance, ~150 km west of the Salt Lake site (Figure 1), the 1990 M_w 5.8 Tianzhu earthquake produced ground cracks along the central Haiyuan Fault, which were recognized in the trenches opened in the epicentral area years later [*Liu-Zeng et al*., 2007]. In addition, *Streig et al*. [2014] reported two paleoseismic events before the 1906 M_w 7.8 earthquake on the Santa Cruz Mountains section of the San Andreas Fault, which were correlative to historical earthquakes of M_w 6.2–6.4 in A.D. 1890 and M_w 7.2 in 1838, respectively.

M 5–6 earthquakes are obviously capable of locally breaking to the surface. The recent example is 20 August 2014 South Napa Valley, California, earthquake of M_w 6.0. This earthquake is associated with 12.5–15 km long surface rupture, with a few to ~50 cm in horizontal slip and small-amplitude mole tracks at surface [*Hudnut et al*., 2014; *Brocher et al*., 2015]. To date, more than two dozen earthquakes worldwide with magnitude 6 and below, in some cases as low as magnitude 3–4, have been reported to have kilometer-long surface ruptures [*Allen and Brune*, 1967; *Wells and Coppersmith*, 1994; *Lettis et al*., 1997; *Berberian et al*., 2001; *Brocher et al*., 2015]. Based on worldwide data set of $M_w > 5$ for the period of 1847–1992, *Wells and Coppersmith* [1993] reported a histogram showing that 80% of earthquakes at M_w 6.7 were accompanied with surface rupture. The probability drops to 50% for M_w 6 and 20% for M_w 5.5 earthquakes, respectively. Recently, *Weldon and Biasi* [2015] presented a conceptual model addressing the probability of paleoseismic detection of ground ruptures as a function of magnitude using constraints from the Wrightwood, California, paleoseismic site. Their analysis suggested a similar probability of 10% for M_w 5, 50–60% for M_w 6.5, and 80% for M_w 7 events, respectively. Thus, the lower the magnitude, the lower the possibility of ruptures reaching the surface, but there is no threshold magnitude for earthquake with surface rupture.

Trenching on a fault is effective in recovering the temporal records of paleoearthquakes, yet difficult to determine their magnitudes or slip. In comparison, *M* 6 earthquakes have rupture length and offset only one tenth of *M* 8 events [*Wells and Coppersmith*, 1994]. With a sequence of such diverse magnitudes, a paleoseismic search for slip-per-event record could easily miss the moderate-magnitude events, as their offsets are similar to the uncertainty in slip measurements.

A number of paleoseismic sites worldwide, with high-resolution stratigraphy, yield long records of past earthquakes [e.g., *Sieh*, 1978a; *Weldon et al*., 2002; *Daëron et al*., 2007; *Berryman et al*., 2012; *Rockwell et al*., 2014]. But whether these sites include only large events or a mixture of large- and moderate-magnitude earthquakes is quite difficult to assess, as in most cases there is no historical records to match. Correlating events between multiple sites along a fault provides constraints on rupture length, but is biased toward favoring long ruptures, especially when sites are several tens of kilometers apart. This could result in an overestimation of event size. Even so, on the San Jacinto Fault, some events recorded at one site do not have correlation at adjacent sites 20–50 km away [*Rockwell et al*., 2014]. Even though it is not a definite proof that these are moderate-magnitude ruptures, they are considerably shorter in extent than some other events, which are correlative over ~100 km distance. Similar pattern of variety in rupture extent emerges from the correlation of ruptures among sites along the southern San Andreas Fault: shorter ruptures appear to be more frequent than the longest ones [*Scharer et al*., 2014].

Our data show that different modes of rupture, corresponding to either large- or moderate-magnitude earthquakes, occurred on the same section of the Haiyuan Fault, as was also observed on other strike-slip faults. Fault patches, which broke in moderate-magnitude events, failed again in large-magnitude M_w 7.8–8.3 earthquakes, after a short interval and as part of the larger multisegment rupture. Hence, the time periods between "large earthquakes" are dotted with moderate-magnitude earthquakes, as shown by the paleoseismological record at our site. To some extent, this could be paralleled with rupture variability in subduction zones, such as the Sumatra [*Sieh et al*., 2008]. Actually, recent paleoseismic results along active continental faults show increasingly that complex earthquake rupture sequences are likely the normal mode and that repetition of earthquake ruptures with similar lateral extent required special conditions [i.e., *Wen et al*., 2008; *Scharer et al*., 2014; *Streig et al*., 2014; *Rockwell et al*., 2014; *Wechsler et al*., 2014]. Hence, derivation of earthquake recurrence intervals solely based on paleoseismic data should be conducted with caution as successive earthquakes recorded at one site will likely be of different magnitude. The proper treatment is to acknowledge the possible range of event size in paleoseismic records explicitly.

9. Conclusions

Paleoseismology provides routinely fundamental data for earthquake recurrence models, by revealing past surface-rupturing events that stopped at different levels in layered soft sediments. Paleoearthquakes recognized in trenches are often unknown in magnitude, vaguely defined as surface-rupturing events, but often explicitly or implicitly assumed to be roughly of a similar magnitude when calculating earthquake recurrence interval in seismic hazard assessment of the studied fault. Recent paleoseismic investigation at the Salt Lake site on the Haiyuan Fault, China, reveals a high-resolution strati-chronology of paleoseismic events, which is directly compared with historical accounts of regional seismicity, providing a unique opportunity to constrain event timing and size. The stratigraphic sequence recorded three, and possibly four, earthquakes since A.D. 1500, constrained by AMS ^{14}C dating. A comparison with regional historical earthquake accounts shows that they are a mix of events of different magnitudes. Except the most recent earthquake of M 8 in 1920, two earlier events, occurred in A.D. 1760 (or 1709) and 1638, respectively, are significantly smaller, with magnitude $M < 7$, possibly M~6.2–6.8 or less. Our study suggests that surface ruptures of local moderate-magnitude earthquakes can be preserved in stratigraphy under favorable conditions. The results thus show that earthquakes with over an order of magnitude difference in rupture length and seismic moment can be recorded at a single site, contrary to the assumption that paleoseismology samples mostly a relatively narrow range of large-magnitude earthquakes. This study points to the need of closely spaced trenches for serious assessment of rupture length and demonstrates the advantage of combining paleoseismic investigation and analyses of historical written records of earthquake shaking to determine earthquake magnitude.

Acknowledgments

This research was supported jointly by China Earthquake Administration (grant 201308012) and the National Science Foundation of China (41172179 and 41225010). Y.K. was partly supported by ANR-05-CATT-0006. Yanfeng Li, Jean-Philippe Adams, Heloise Beurdouche, Xiucheng Xing, and Jingyu Zhang contributed in the field work. Austin Elliott carried out laboratory work for a subset of charcoal samples. Arizona AMS Laboratory, UC Irvine Keck Carbon Cycle AMS Facility, and University of Glasgow produced jointly radiocarbon analyses. We thank Katherine Scharer and Michael Oskin for their careful and thorough reviews, Editor Michael Walter for the editorial help, David Schwartz for commenting on earlier version of this manuscript, and Zhigang Li for helping with restoration of event deformation. All data for this paper are properly cited and referred to in the reference list.

References

Abe, K. (1981), Magnitudes of large shallow earthquakes from 1904 to 1980, *Phys. Earth Planet. Inter.*, *27*, 72–92.

Akciz, S., L. Ludwig, J. Arrowsmith, and O. Zielke (2010), Century-long average time intervals between earthquake ruptures of the San Andreas Fault in the Carrizo Plain, California, *Geology*, *38*, 787–790.

Allen, C. R. (1986), Seismological and paleoseismological techniques of research in active tectonics, in *Active Tectonics*, edited by R. E. Wallace, pp. 148–154, Natl. Acad. Press, Washington, D. C.

Allen, C. R., and J. N. Brune (1967), A low-stress-drop, low-magnitude earthquake with surface faulting: The Imperial, California, earthquake of March 4, 1966, *Bull. Seismol. Soc. Am.*, *57*, 501–514.

Ambraseys, N. N. (2009), *Earthquakes in the Mediterranean and Middle East: A Multidisciplinary Study of Seismicity Up to 1900*, 947 pp., Cambridge Univ. Press, Cambridge, U. K.

Avouac, J., and P. Tapponnier (1993), Kinematic model of active deformation in central Asia, *Geophys. Res. Lett.*, *20*, 895–898, doi:10.1029/93GL00128.

Bakun, W. H., and C. M. Wentworth (1997), Estimating earthquake location and magnitude from seismic intensity data, *Bull. Seismol. Soc. Am.*, *87*, 1502–1521.

Berberian, M., J. Jackson, E. Fielding, B. Parsons, K. Priestley, M. Qorashi, M. Talebian, R. Walker, T. Wright, and C. Baker (2001), The 1998 March 14 Fandoqa earthquake (M_w 6.6) in Kerman Province, southeast Iran: Re-rupture of the 1981 Sirch earthquake fault, triggering of slip on adjacent thrusts and the active tectonics of the Gowk fault zone, *Geophys. J. Int.*, *146*, 371–398.

Berryman, K., U. Cochran, K. Clark, G. Biasi, R. Langridge, and P. Villamor (2012), Major earthquakes occur regularly on an isolated plate boundary fault, *Science*, *336*, 1690–1693.

Bonilla, M. G., and J. J. Lienkaemper (1990), Visibility of fault strands in exploratory trenches and timing of rupture events, *Geology*, *18*, 153–156.

Brocher, M. T., et al. (2015), The M_w 6.0 24 August 2014 South Napa earthquake, *Seismol. Res. Lett.*, *86*, 309–326, doi:10.1785/0220150004.

Bronk Ramsey, C. (2013), OxCal 4.2 manual, Oxford Radiocarbon Accelerator Unit. [Available at https://c14.arch.ox.ac.uk/oxcalhelp/hlp_contents.html.]

Burchfiel, B. C., P. Zhang, Y. Wang, W. Zhang, P. Molnar, and L. Royden (1991), Geology of the Haiyuan fault zone, Ningxia-Hui Autonomous Region, China and its relation to the evolution of the northeastern of the Tibetan Plateau, *Tectonics*, *10*, 1091–1110, doi:10.1029/90TC02685.

Cai, Z., W. Zhang, and D. Jiao (1997), Discussion of the level active severity in different time intervals and segments on late Quaternary along Tianjingshan fault zone [in Chinese with English abstract], *Earthquake Res. China*, *13*(1), 35–42.

Cavalié, O., C. Lasserre, M. P. Doin, G. Peltzer, J. Sun, X. Xu, and Z. Shen (2008), Measurement of interseismic strain across the Haiyuan Fault (Gansu, China), by InSAR, *Earth Planet. Sci. Lett.*, *275*(3/4), 246–257, doi:10.1016/j.epsl.2008.07.057.

Central Office of Earthquake Working Group (1971), *Catalogue of Chinese Earthquakes* [in Chinese], *Book Ser. I to IV*, Science, Beijing.

Chen, T., P. Zhang, J. Liu, C. Li, Z. Ren, and K. Hudnut (2014), Quantitative study of tectonic geomorphology along Haiyuan Fault based on airborne LiDAR, *Chin. Sci. Bull.*, *59*(20), 2396–2409, doi:10.1007/s11434-014-0199-4.

Chen, W. P., and P. Molnar (1977), Seismic moments of major earthquakes and average rate of slip in central Asia, *J. Geophys. Res.*, *82*, 2954–2969.

Close, U., and E. McCormick (1922), Where the mountains walked, *Natl. Geogr. Mag.*, *12*(5), 445–464.

Committee of Earthquake Research, Academia Sinica (1956), *Chronical Data of Chinese Historical Earthquakes* [in Chinese], *Book Ser. I & II*, Science, Beijing.

Daëron, M., Y. Klinger, P. Tapponnier, A. Elias, E. Jacques, and A. Sursock (2007), 12,000-year-long record of up to 14 paleo-earthquakes on the Yammoûneh Fault (Levant fault system), *Bull. Seismol. Soc. Am.*, *97*, 749–771.

Deng, Q., S. Chen, F. Song, S. Zhou, Y. Wang, W. Zhang, and P. Zhang (1986), Variations in the geometry and amount of slip on the Haiyuan (Nanxihaushan) fault zone, China and the surface rupture of the 1920 Haiyuan earthquake, in *Earthquake Source Mechanics*, pp. 169–182, AGU, Washington, D. C.

Ding, G., J. Chen, Q. Tian, X. Shen, C. Xing, and K. Wei (2004), Active faults and magnitudes of left-lateral displacement along the northern margin of the Tibetan Plateau, *Tectonophysics*, *380*, 243–260.

Division of Earthquake Monitoring and Prediction, State Seismologic Bureau (DEMPSSB) (1995), *Catalog of Chinese Historical Strong Earthquakes (2300 B.C.–1911 A.D.), China*, 514 pp., Seismol. Press, Beijing.

Duvall, A. R., and M. Clark (2010), Dissipation of fast strike-slip faulting within and beyond northeastern Tibet, *Geology*, *38*(3), 223–226.

Field, E. H., et al. (2014), Uniform California Earthquake Rupture Forecast, version 3 (UCERF3)—The time-independent model, *Bull. Seismol. Soc. Am.*, *104*(3), 1122–1180.

Gaudemer, Y., P. Tapponnier, B. Meyer, G. Peltzer, S. Guo, Z. Chen, H. Dai, and I. Cifuentes (1995), Partitioning of crustal slip between linked active faults in the eastern Qilian Shan and evidence for a major seismic gap, the "Tianzhu gap," on the western Haiyuan Fault, Gansu (China), *Geophys. J. Int.*, *120*, 599–645.

Grant-Ludwig, L., S. O. Akçiz, G. R. Noriega, O. Zielke, and J. R. Arrowsmith (2010), Climate-modulated channel incision and rupture history of the San Andreas Fault in the Carrizo Plain, *Science*, *27*, 1117–1119, doi:10.1126/science.1182837.

Gu, G. (1983), *Catalogue of Chinese Earthquakes (1831 B.C.–1969 A.D.)* [in Chinese], Science, Beijing.

He, W., B. Liu, T. Lu, D. Yuan, J. Liu, and X. Liu (1994), Study on the segmentation of Laohushan fault zone [in Chinese with English abstract], *Northwest. Seismol. J.*, *16*, 66–72.

He, W., B. Liu, T. Lu, D. Yuan, and X. Liu (1996), The late Quaternary activity of the Maomaoshan fault zone [in Chinese with English abstract], in *Research on Active Fault Series 5*, edited by Q. Deng, Y. Wang, and P. Zhang, pp. 63–77, Seismol. Press, Beijing.

Hudnut, K. W., L. Seeber, and J. Pacheco (1989), Cross-fault triggering in the November 1987 Superstition Hills Earthquake Sequence, southern California, *Geophys. Res. Lett.*, *16*, 199–202.

Hudnut, K. W., et al. (2014), Key recovery factors for the August 24, 2014, South Napa earthquake, *U.S. Geol. Surv. Open-File Rep. 1249*, 51 pp., doi:10.3133/ofr20141249.

Institute of Geology, China Earthquake Administration (IGCEA), and Ninxia Bureau of China Earthquake Administration (NBCEA) (1990), *Active Haiyuan Fault Zone Monograph*, *Spec. Publ. on Active Fault Stud. in China* [in Chinese], 286 pp., Seismol. House, Beijing.

Institute of Geophysics, China Earthquake Administration (IGCEA), and Institute of Historic Geography, Fudan University (HGFU) (1986), *Atlas of the Historic Earthquakes in China, the Ming Dynasty Period* [in Chinese], 194 pp., China Cartogr. House, Beijing.

Institute of Geophysics, China Earthquake Administration (IGCEA), and Institute of Historic Geography, Fudan Univ. (HGFU) (1990), *Atlas of the Historic Earthquakes in China, the Qing Dynasty Period* [in Chinese], 244 pp., China Cartogr. House, Beijing.

Jolivet, R., C. Lasserre, M. P. Doin, S. Guillaso, G. Peltzer, R. Dailu, J. Sun, Z. Shen, and X. Xu (2012), Shallow creep on the Haiyuan Fault (Gansu, China) revealed by SAR interferometry, *J. Geophys. Res.*, *117*, B06401, doi:10.1029/2011JB008732.

Klinger, Y. (2010), Relation between continental strike-slip earthquake segmentation and thickness of the crust, *J. Geophys. Res.*, *115*, B07306, doi:10.1029/2009JB006550.

Klinger, Y., M. L. Béon, and M. Al-Qaryouti (2015), 5000 yr of paleoseismicity along the southern Dead Sea fault, *Geophys. J. Int.*, *202*, 313–327.

Klinger, Y., M. Etchebes, P. Tapponnier, and C. Narteau (2011), Characteristic slip for five great earthquakes along the Fuyun Fault in China, *Nat. Geosci.*, *4*, 389–392, doi:10.1038/ngeo1158.

Kondo, H., V. Özaksoy, and C. Yıldirim (2010), Slip history of the 1944 Bolu-Gerede earthquake rupture along the North Anatolian fault system: Implications for recurrence behavior of multisegment earthquakes, *J. Geophys. Res.*, *115*, B04316, doi:10.1029/2009JB006413.

Lanzhou Institute of Earthquake Research (LIER) (1989), *Data Compilation of Historical Earthquakes in Gansu* [in Chinese], 618 pp., Seismol. Press, Beijing, China.

Lanzhou Institute of Seismology (LIS), and Ningxia Bureau of China Earthquake Administration (NBCEA) (1980), *The Haiyuan Earthquake in 1920* [in Chinese], Seismol. House, Beijing.

Lasserre, C., et al. (1999), Postglacial left slip rate and past occurrence of $M \geq 8$ earthquakes on the western Haiyuan Fault, Gansu, China, *J. Geophys. Res.*, *104*, 17,633–17,652, doi:10.1029/1998JB900082.

Lasserre, C., Y. Gaudemer, P. Tapponnier, A.-S. Me'riaux, J. Van der Woerd, D. Yuan, F. J. Ryerson, R. C. Finkel, and M. W. Caffee (2002), Fast late Pleistocene slip rate on the Leng Long Ling segment of the Haiyuan Fault, Qinghai, China, *J. Geophys. Res.*, *107*(B11), 2276, doi:10.1029/2000JB000060.

Lettis, W. R., D. L. Wells, and J. N. Baldwin (1997), Empirical observations regarding reverse earthquakes, blind thrust faults, and quaternary deformation: Are blind thrust faults truly blind?, *Bull. Seismol. Soc. Am.*, *87*(5), 1171–1198.

Li, C., P. Zhang, J. Yin, and W. Min (2009), Late Quaternary left-lateral slip rate of the Haiyuan Fault, northeastern margin of the Tibetan Plateau, *Tectonics*, *28*, TC5010, doi:10.1029/2008TC002302.

Li, S. B. (Ed.) (1960), *Catalogue of Chinese Earthquakes (1831 B.C.–1969 A.D.)* [in Chinese], Seismol. Press, Beijing.

Liu, B., J. Zhang, J. Wu, and H. Guo (2003), Reevaluating on casualty in the Haiyuan M_S 8.5 earthquake on December 16, 1920, *Earthquake Res. China*, *19*(4), 386–399.

Liu, Y., A. Wang, Y. Li, H. Liu, and Y. Zhang (2006), Research on active features and tectonic stability in the late Quaternary of the Northern Piedmont Fault of Changlingshan [in Chinese with English abstract], *Earthquake Res. China*, *22*(4), 394–404.

Liu-Zeng, J., Y. Klinger, K. Sieh, C. Rubin, and G. Seitz (2006), Serial ruptures of the San Andreas Fault, Carrizo Plain, California, revealed by three-dimensional excavations, *J. Geophys. Res.*, *111*, B02306, doi:10.1029/2004JB003601.

Liu-Zeng, J., Y. Klinger, X. Xu, C. Lasserre, G. Chen, W. Chen, P. Tapponnier, and B. Zhang (2007), Millennial recurrence of large earthquakes on the Haiyuan Fault near Songshan, Gansu Province, China, *Bull. Seismol. Soc. Am.*, *97*, 14–34.

Marco, S., M. Stein, and A. Agnon (1996), Long-term earthquake clustering: A 50,000-year paleoseismic record in the Dead Sea Graben, *J. Geophys. Res*, *101*(B3), 6179–6191.

Marco, S., A. Agnon, R. Ellenblum, A. Eidelman, U. Basson, and A. Boas (1997), 817-year-old walls offset sinistrally 2.1 m by the Dead Sea Transform, Israel, *J. Geodyn.*, *24*, 11–20.

McCalpin, J. P. (2009), *Paleoseismology*, 2nd ed., Elsevier, Oxford, U. K.

McGill, S. F., and K. Sieh (1991), Surficial offsets on the Central and Eastern Garlock Fault associated with prehistoric earthquakes, *J. Geophys. Res.*, *96*, 21,597–21,621, doi:10.1029/91JB02030.

Min, W., P. Zhang, Q. Deng, and F. Mao (2001), Detailed study of Holocene paleoearthquakes of the Haiyuan active fault, *Geol. Rev.*, *47*(1), 75–81.

National Quality and Technology Supervision Administration (NQTSA) (1999), The Chinese seismic intensity scale, GB/T 17742-1999, National Standard in the People's Republic of China.

Nie, Z., and W. Lin (1993), Middle segment of Zhongwei-Tongxin fault zone: Seismic deformation band of 1709 earthquake with $M = 7½$ Xiangshan-Tianjingshan fault zone [in Chinese with English abstract], *Earthquake*, *1*, 41–44.

Ningxia Bureau of China Earthquake Administration (NBCEA) (1988), *Data Compilation of Historical Earthquakes in Ningxia* [in Chinese], 343 pp., Seismol. Press, Beijing, China.

Nishenko, S. P., and R. Buland (1987), A generic recurrence interval distribution for earthquake forecasting, *Bull. Seismol. Soc. Am.*, *77*, 1,382–1,399.

Peltzer, G., and P. Tapponnier (1988), Formation and evolution of strike-slip faults, rifts, and basins during the India-Asia collision: An experimental approach, *J. Geophys. Res.*, *93*, 15,085–15,117, doi:10.1029/JB093iB12p15085.

Ran, Y., R. Duan, and Q. Deng (1997), 3-D trench excavation and paleoseismology at Gaowanzi of the Haiyuan Fault [in Chinese with English abstract], *Earthquake Geol.*, *19*(2), 97–107.

Reimer, P. J., et al. (2009), IntCal09 and Marine09 radiocarbon age calibration curves, 0–50,000 years cal B.P, *Radiocarbon*, *51*, 1111–1150.

Richter, F. R. (1958), *Elementary Seismology*, W. H. Freeman, San Francisco, Calif.

Rockwell, T. K., R. S. McElwain, D. E. Millman, and D. L. Lamar (1986), Recurrent late Holocene faulting on the Glen Ivy north strand of the Elsinore Fault at Glen Ivy marsh, *Guidebook and Volume on Neotectonics and Faulting in Southern California*, edited by P. Ehlig, pp. 167–176, *Cordilleran Sect.*, Geol. Soc. of Am.

Rockwell, T. K., T. E. Dawson, J. Y. Ben-Horin, and G. Seitz (2014), A 21-event, 4,000-year history of surface ruptures in the Anza seismic gap, San Jacinto Fault, and implications for long-term earthquake production on a major plate boundary fault, *Pure Appl. Geophys.*, *172*(5), 1143–1165.

Romeo, R. W. (2005), Earthquake Hazard in Italy, 2001–2030, *Nat. Hazard*, *36*, 383–405.

Rymer, M. J., J. Boatwright, L. C. Seekins, J. D. Yule, and J. Liu (2002), Triggered Surface Slips in the Salton Trough Associated with the 1999 Hector Mine, California, Earthquake, *Bull. Seis. Soc. Am.*, *92*, 1300–1317.

Rymer, M. J., et al. (2010), Triggered surface slips in southern California associated with the 2010 El Mayor-Cucapah, Baja California, Mexico, earthquake, *U.S. Geol. Surv. Open File Rep.*, 2010–1333.

Sapkota, S. N., L. Bollinger, Y. Klinger, P. Tapponnier, Y. Gaudemer, and D. Tiwar (2012), Primary surface ruptures of the great Himalayan earthquakes in 1934 and 1255, *Nat. Geosci.*, *6*, 71–76.

Scharer, K., R. Weldon II, A. Streig, and T. Fumal (2014), Paleoearthquakes at Frazier Mountain, California delimit extent and frequency of past San Andreas Fault ruptures along 1857 trace, *Geophys. Res. Lett.*, *41*, 4527–4534, doi:10.1002/2014GL060318.

Scharer, K. M., R. J. Weldon, T. E. Fumal, and G. P. Biasi (2007), Paleoearthquakes on the southern San Andreas Fault, Wrightwood, CA 3000 to 1500 B.C.: A new method for evaluating paleoseismic evidence and earthquake horizons, *Bull. Seismol. Soc. Am.*, *97*, 1054–1093.

Scholz, C. H. (1982), Scaling laws for large earthquakes: Consequences for physical models, *Bull. Seismol. Soc. Am.*, *72*(1), 1–14.

Schwartz, D. P., and K. J. Coppersmith (1984), Fault behavior and characteristic earthquakes: Examples from the Wasatch and San Andreas fault zones, *J. Geophys. Res.*, *89*, 5681–5698, doi:10.1029/JB089iB07p05681.

Sieh, K. E. (1978a), Prehistoric large earthquakes produced by slip on the San Andreas Fault at Pallett Creek, California, *J. Geophys. Res.*, *83*, 3907–3939, doi:10.1029/JB083iB08p03907.

Sieh, K. E. (1978b), Slip along the San Andreas Fault associated with the great 1857 earthquake, *Bull. Seismol. Soc. Am.*, *68*, 1421–1448.

Sieh, K. E. (1996), The repetition of large-earthquake ruptures, *Proc. Natl. Acad. Sci. U.S.A.*, *93*, 3764–3771.

Sieh, K. E., D. H. Natawidjaja, A. J. Meltzner, C.-C. Shen, H. Cheng, K.-S. Li, B. W. Suwargadi, J. Galetzka, B. Philibosian, and R. L. Edwards (2008), Earthquake supercycles inferred from sea-level changes recorded in the corals of west Sumatra, *Science*, *322*(5908), 1674–1678.

Streig, A. R., T. E. Dawson, and R. J. Weldon II (2014), Paleoseismic evidence of the 1890 and 1838 earthquakes on the Santa Cruz Mountains section of the San Andreas Fault, near Corralitos, California, *Bull. Seismol. Soc. Am.*, *104*(1), 285–300, doi:10.1785/0120130009.

Stuiver, M., and H. A. Polach (1977), Discussion: Reporting of ^{14}C data, *Radiocarbon*, *19*(3), 355–363.

Tapponnier, P., Z. Xu, F. Roger, B. Meyer, N. Arnaud, G. Wittlinger, and J. Yang (2001), Oblique stepwise rise and growth of the Tibet Plateau, *Science*, *294*(5547), 1671–1677.

Wechsler, N., T. K. Rockwell, Y. Klinger, P. Stepancikova, M. Kanari, S. Marco, and A. Agnon (2014), A paleoseismic record of earthquakes for the Dead Sea transform fault between the first and seventh centuries C.E.: Nonperiodic behavior of a plate boundary fault, *Bull. Seismol. Soc. Am.*, *104*(3), 1329–1347.

Wei, M., D. Sandwell, Y. Fialko, and R. Bilham (2011), Slip on faults in the Imperial Valley triggered by the 4 April 2010 M_w 7.2 El Mayor-Cucapah earthquake revealed by InSAR, *Geophys. Res. Lett.*, *38*, L01308, doi:10.1029/2010GL045235.

Weldon, R.J. II and G. Biasi (2015), Probability of detection of ground rupture at paleoseismic sites, Appendix I, Uniform California Earthquake Rupture Forecast, Version 3 (UCERF3).

Weldon, R. J., II, T. E. Fumal, T. J. Powers, S. K. Pezzopane, K. M. Scharer, and J. C. Hamilton (2002), Structure and earthquake offsets on the San Andreas Fault at the Wrightwood, California, paleoseismic site, *Bull. Seismol. Soc. Am.*, *92*(7), 2704–2725.

Weldon, R. J., II, K. Scharer, T. Fumal, and G. Biasi (2004), Wrightwood and the earthquake cycle: What a long recurrence record tells us about how faults work, *GSA Today*, *14*(9), 4–10.

Wells, D. L., and K. J. Coppersmith (1993), Likelihood of surface rupture as a function of magnitude, *Seismol. Res. Lett.*, *64*(1), 54.

Wells, D. L., and K. J. Coppersmith (1994), New empirical relationships among magnitude, rupture length, rupture width, rupture area, and surface displacement, *Bull. Seismol. Soc. Am.*, *84*, 974–1002.

Wen, X., S. Ma, X. Xu, and Y. He (2008), Historical pattern and behavior of earthquake ruptures along the eastern boundary of the Sichuan-Yunnan faulted-block, southwestern China, *Phys. Earth Planet. Inter.*, *168*, 16–36.

Wesnousky, S. G. (2006), Predicting the endpoints of earthquake ruptures, *Nature*, *444*, 358–360, doi:10.1038/nature05275.

Wesnousky, S. G. (2008), Displacement and geometrical characteristics of earthquake surface ruptures: Issues and implications for seismic hazard analysis and the earthquake rupture process, *Bull. Seismol. Soc. Am.*, *98*(4), 1609–1632.
Working Group on California Earthquake Probabilities (WGCEP) (1995), Seismic hazards in Southern California: Probable earthquakes, 1994–2024, *Bull. Seismol. Soc. Am.*, *85*, 379–439.
Working Group on California Earthquake Probabilities (WGCEP) (2003), Earthquake probabilities in the San Francisco Bay area, *U. S. Geol. Surv. Open File Rep., 2003-214,* 235 pp.
Xie, Y. S., and M. B. Cai (Eds.) (1983), *Compilation of Historical Materials of Chinese Earthquakes*, *From Remote Antiq. to the Yuan Dynasty* [in Chinese], vol. I, Science, Beijing.
Xie, Y. S., and M. B. Cai (Eds.) (1985), *Compilation of Historical Materials of Chinese Earthquakes*, *The Ming Dynasty* [in Chinese], vol. II, Science, Beijing.
Xie, Y. S., and M. B. Cai (Eds.) (1987a), *Compilation of Historical Materials of Chinese Earthquakes* [in Chinese], *The Qing Dynasty-1*, vol. III, Science, Beijing.
Xie, Y. S., and M. B. Cai (Eds.) (1987b), *Compilation of Historical Materials of Chinese Earthquakes* [in Chinese], *The Qing Dynasty-2*, vol. III, Science, Beijing.
Yeats, R. S., K. Sieh, and C. R. Allen (1997), The Geology of Earthquakes, Oxford Univ. Press, New York.
Yin, G., Y. Jiang, and G. Yu (2013), The study of the left-lateral displacement on the Xiangshan-Tianjingshan Fault in late Quaternary, *Seismol. Geol.*, *35*(3), 472–479.
Yuan, D., B. Liu, T. Lu, W. He, X. Liu, and W. Gan (1998), Study on the segmentation in east segment of the northern Qilianshan fault zone [in Chinese with English abstract], *Northwest. Seismol. J.*, *20*, 27–34.
Yuan, D., Z. Lei, W. He, Z. Xiong, W. Ge, X. Liu, and B. Liu (2007), Textural research of Wudu earthquake in 186 B.C. in Gansu Province, China and discussion on its causative structure [in Chinese with English abstract], *Acta Seismol. Sin.*, *29*, 644–663.
Zhang, P., P. Molnar, B. C. Burchfiel, L. Royden, W. Zhang, D. Jiao, Q. Deng, Y. Wang, and F. Song (1988a), Bounds on the recurrence interval of major earthquakes along the Haiyuan fault in north-central China, *Seismol. Res. Lett.*, *59*, 81–89.
Zhang, P., P. Molnar, B. C. Burchfiel, L. Royden, W. Zhang, D. Jiao, Q. Deng, Y. Wang, and F. Song (1988b), Bounds on the Holocene slip rate along the Haiyuan Fault, north-central China, *Quat. Res.*, *30*, 151–164.
Zhang, P., B. C. Burchfield, S. Chen, and Q. Deng (1989), Extinction of pull-apart basins, *Geology*, *17*, 814–817.
Zhang, P., W. Min, Q. Deng, and F. Mao (2003), Paleoearthquake rupture behavior and recurrence of great earthquakes along the Haiyuan Fault, northwestern China, *Sci. China, Ser. D*, *46*, 705–713.
Zhang, W. (Ed.) (1934), *History of Evolving Townships of the Gansu Province in Maps and Tables* [in Chinese], 155 pp., Peking, China.
Zhang, W., D. Jiao, P. Zhang, P. Molnar, B. C. Burchfield, Q. Deng, Y. Wang, and F. Song (1987), Displacement along the Haiyuan Fault associated with the great 1920 Haiyuan China earthquake, *Bull. Seismol. Soc. Am.*, *77*, 117–131.
Zhang, W., D. Jiao, Z. Cai, F. Song, and Y. Wang (1988), Neotectonic features of the Xiangshan-Tianjinshang arc fracture zone and the seismic deformation zone of 1709 south of Zhongwei $M = 7½$ earthquake [in Chinese with English abstract], *Seismol. Geol.*, *10*(3), 12–20.
Zhou, J., and B. Liu (1987), The research of active Zhongwei-Tongxin Fault [in Chinese with English abstract], *Northwest. Seismol. J.*, *9*(3), 71–77.
Zielke, O., J. R. Arrowsmith, L. Grant Ludwig, and S. O. Akçiz (2010), Slip in the 1857 and earlier large earthquakes along the Carrizo Plain, San Andreas Fault, *Science*, *327*, 1119–1121, doi:10.1126/science.1182781.